Available online at www.sciencedirect.com
ScienceDirect
Journal of Volcanology and Geothermal Research 168 (2007) 28–54
Journal of volcanology and geothermal research
www.elsevier.com/locate/jvolgeores

Insights into magmatic evolution and recharge history in Capraia Volcano (Italy) from chemical and isotopic zoning in plagioclase phenocrysts

D. Gagnevin [a,*], T.E. Waight [b], J.S. Daly [a], G. Poli [c], S. Conticelli [d]

[a] *School of Geological Sciences, University College Dublin, Belfield, Dublin 4, Ireland*
[b] *Institute for Geography and Geology, Øster Voldgade 10, 1350 Copenhagen K, Denmark*
[c] *Department of Earth-Sciences, Piazza Universitá, 06100 Perugia, Italy*
[d] *Dipartimento di Scienze della Terra, Universita degli Studi di Firenze, Via La Pira, 4, I-50121 Firenze, Italy*

Received 20 December 2006; accepted 20 July 2007
Available online 15 August 2007

Abstract

Plagioclase phenocrysts in dacites from the high-K calc-alkaline Capraia Volcano were investigated for major, trace element and Sr isotope variations in order to gain better insight into the proposed open-system behaviour of the volcano. Repeated dissolution zones in plagioclases from the early-erupted Monte Castello (MC) and later Monte Rucitello (MR) dacitic units are associated with a sharp increase in An content and variation in isotopic compositions ($^{87}Sr/^{86}Sr = 0.70872–0.71004$), which argue for repeated magma mixing. In particular, petrographic and mineralogical evidence suggest that recharge with hot, basaltic magma occurred repeatedly during the lifetime of the Capraia volcanic system. We attempted to correlate shared crystallization and resorption histories using chemical (mol% An, Fe) and Sr isotopic zoning in plagioclase. In this correlation framework, the observed mismatch between chemical and isotopic data in some phenocrysts is interpreted to reflect either growth of phenocrysts in a separate magma chamber, or compositional zoning within a single magma chamber. A minor role of crustal contamination is inferred. Instead, the intra-crystal variations in isotopic composition in plagioclase reflect the existence of distinct components that may have thoroughly mixed at the end of the MC plagioclase growth history. The dominant radiogenic component is similar to lamproites occurring in Tuscany. Recharge with this component occurred throughout the genesis of the MR dacites, but was restricted to the early growth history of the MC dacites. The MR plagioclases are inferred to have crystallized from separate, more differentiated batches of magma that were likely to have evolved at the top of a zoned magma reservoir. Decrease in the An content after most dissolution zones in all phenocrysts, and low temperature estimates from zircon saturation thermometry (<800 °C) also emphasize the importance of crystal fractionation during the evolution of the volcano, in agreement with the occurrence of a significant amount of rhyolitic material. Thus, it is inferred that a rather large magma chamber may have existed during the first cycle of eruptive activity.
© 2007 Elsevier B.V. All rights reserved.

Keywords: Capraia; magma recharge; resorption; electron probe; microsampling; isotopes; fractionation

* Corresponding author. Tel.: +353 1716 2326; fax: +353 1283 7733.
E-mail address: Damien.Gagnevin@ucd.ie (D. Gagnevin).

0377-0273/$ - see front matter © 2007 Elsevier B.V. All rights reserved.
doi:10.1016/j.jvolgeores.2007.07.018

1. Introduction

Magma mixing between mafic (basaltic to trachy-basaltic) and silicic (dacitic to rhyolitic) magmas has often been invoked for the genesis of lavas in calc-alkaline volcanoes (Thompson and Dungan, 1985; Feeley et al., 1998; Clynne, 1999; Schmitt et al., 2001; Izbekov et al., 2002; Price et al., 2005). When such open-system processes are involved, both textural and geochemical evidence in phenocrysts attests to extensive and repeated mineral-melt reactions (Kuscu and Floyd, 2001; Browne et al., 2006), in agreement with, and further constraining, the large chemical and isotopic variations observed for a given suite of hybrid rocks (e.g., Feeley and Dungan, 1996). In particular, chemical and isotopic zoning in plagioclase phenocrysts has been shown to be a powerful petrogenetic tool in deciphering both magmatic processes and their timescales in volcanic (e.g., Davidson and Tepley, 1997; Tepley et al., 1999, 2000) and plutonic (e.g., Waight et al., 2000; Gagnevin et al., 2005a,b) environments. With the aid of experimental data (e.g., Tsuchiyama, 1985), plagioclase major and trace element zoning has been used to demonstrate processes such as magma mixing/recharge (e.g., Schmitt et al., 2001; Izbekov et al., 2002; Zellmer et al., 2003; Gioncada et al., 2005; Browne et al., 2006; Triebold et al., 2006) and/or closed-system crystal fractionation (e.g., Singer et al., 1993; Brophy et al., 1996; Barbey et al., 2005), sometimes combined together (Blundy and Shimizu, 1991; Singer et al., 1995; Ginibre et al., 2002; Francalanci et al., 2005).

The promising aspect of using trace and minor elements in plagioclase is their various sensitivity to both intensive parameters (P, T, $X\mathrm{H_2O}$) and melt compositions during growth (Ginibre et al., 2002; Francalanci et al., 2005). Chemical zoning in pyroxene phenocrysts also mirrors chemical variations in the melt (Shimizu and Le Roex, 1986), and has been used as a tool to decipher petrogenesis and magma chamber dynamics during magma mixing (Umino and Horio, 1998).

Magma mixing between crustal and mantle-derived melts has often been proposed for the genesis of Tuscan magmas (e.g., Giraud et al., 1986; Poli, 1992; Innocenti et al., 1992), including, amongst others, the San Vincenzo rhyolites (Feldstein et al., 1994), the Monte Amiata trachy-dacites (Van Bergen, 1985), and the Monte Capanne monzogranite, Elba Island (Fig. 1; Dini et al., 2002; Gagnevin et al., 2004). In some cases, isotopic and trace element microanalyses of minerals support mixing as a prime process during petrogenesis (Feldstein et al., 1994; Gagnevin et al., 2005a,b), with the net advantage compared to a whole-rock approach of better constraining the changes in magma composition in time, ultimately linked to magma chamber dynamics. In this contribution, with the aid of whole-rock and pyroxene geochemical data, we use plagioclase as a proxy for the petrogenetic evolution of the Capraia Volcano. Detailed BSE images are coupled with chemical and isotopic analyses of plagioclase phenocrysts, which allow us to distinguish growth and dissolution zones, thus better constraining the open-system history of the volcano.

2. Geological setting and geochemistry

The Capraia Volcano (c. 20 km^2) is part of the Tuscan Magmatic Province (TMP), and is situated offshore of the Italian mainland, north of the Elba plutonic complex (Fig. 1). Tuscan magmatism is composed of both plutonic and volcanic rocks in nearly equal proportions, although their geographic distribution is well defined, i.e. most of the plutonic rocks are in the west in the Tuscan Archipelago, while most of the volcanic rocks are in the east on the Italian mainland. Capraia constitutes the only volcanic edifice within the Tuscan Archipelago (Fig. 1). Magmatism in the TMP has been attributed to subduction of the Adriatic plate (Conticelli and Peccerillo, 1992; Serri et al., 1993) and progressive slab roll-back (Brunet et al., 2000), resulting in extensional deformation and melting of upwelling asthenospheric and overlying lithospheric mantle. Metasomatism of the lithospheric mantle source resulted in a wide variety of magmatic products (from calc-alkaline, shoshonitic to lamproitic magmas; Innocenti et al., 1992; Serri et al., 1993; Peccerillo, 1999; Conticelli et al., 1992, 2002).

Capraia Volcano is mainly composed of lava flows, domes and pyroclastic deposits that were erupted between 7.25 and 7.59 Ma (K–Ar ages), defining the first cycle of eruptive activity (Aldighieri et al., 1998). After a gap of *c.* 3 Ma, lava flows and a trachy-basaltic neck (4.65 Ma; K–Ar age) were erupted in the extreme south of the island (Fig. 1; Aldighieri et al., 1998). Field relationships suggest that the strato-volcano suffered two major lateral collapses on the eastern flank, which were followed by renewed eruptive activity, thus defining a crude stratigraphy. The Monte Rosso and the Monte Castello (MC) are the oldest andesitic/dacitic units, while the Monte Rucitello (MR) dacites end the first eruptive cycle, with eruptions of the Monte Campanile and the Monte Albero dacites in between (Fig. 1). In the field, compositional banding and/or minor mafic inclusions (Fig. 2a) are common.

Geochemical overviews of the Capraia lavas are presented in Prosperini (1993) and Poli and Perugini (2003). Most of the lavas in Capraia range in composition

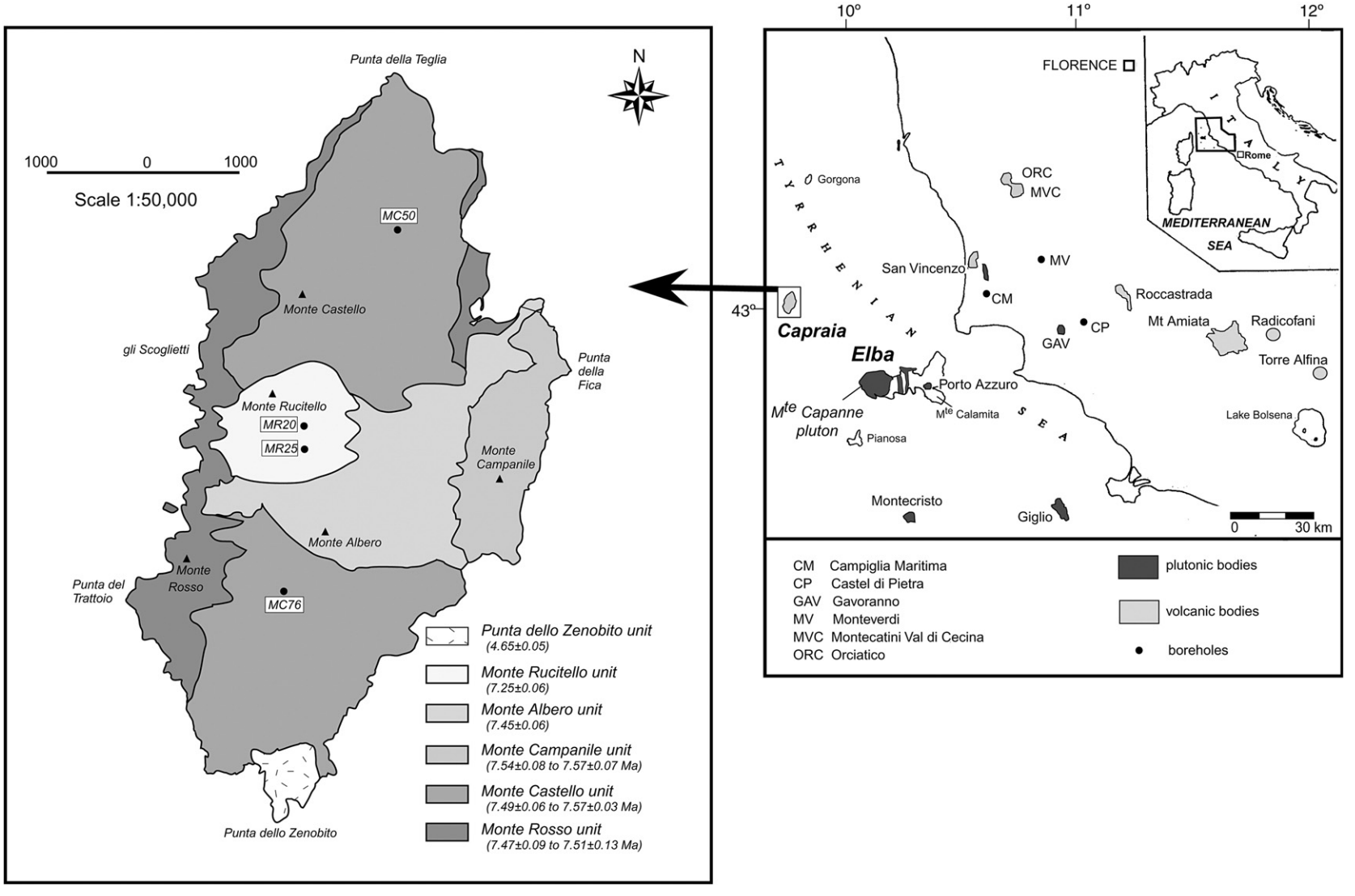

Fig. 1. Map of the Tuscan Magmatic Province and geological map of Capraia Island (adapted from Aldighieri et al., 1998) showing sample localities as labeled filled circles. The grey shading indicates the stratigraphic order for the first cycle of eruptive activity (K–Ar data; Aldighieri et al., 1998), from older (dark grey = Monte Rosso unit) to younger (light grey = Monte Rucitello) units. The Punta dello Zenobito system (4.65 Ma) represents the second cycle of eruptive activity and mostly consists of basaltic lavas.

from andesites, dacites and rhyolites, with a predominant high-K calc-alkaline signature, apart from the last erupted Zenobito trachy-basalts (4.65 Ma) that have shoshonitic affinities, a feature common in the younger (0.05–1.40 Ma) Roman Magmatic Province (Conticelli and Peccerillo, 1992). The first cycle of eruptive activity (>7 Ma) consists exclusively of differentiated lavas (dacites and subordinate andesites). All lavas are enriched in K_2O (2.5–4.0 wt.%) and LREE and lack primary compositions (maximum Cr and Ni contents of 412 ppm and 91 ppm, respectively). A combined mixing and fractional crystallization (MFC; Poli, 1992) petrogenetic model has been envisaged by Poli and Perugini (2003) to account for the bulk chemical composition of the Capraia lavas, which includes mixing between various mantle-derived end-members (high-K andesitic, lamproitic and shoshonitic). In particular, mixing involving high-K andesitic and lamproitic magmas is thought to be an important process in the genesis of the lavas. Variable initial whole rock Sr isotopic compositions (from 0.7072 to 0.7102; Poli and Conticelli, unpublished data) are consistent with an open-system model for the genesis of the Capraia lavas. Arguably, the absence of crustal xenoliths and/or xenocrysts (garnet, cordierite, etc.), as well as relatively unradiogenic Sr isotopic compositions of the lavas (<0.7105) compared to typical crustal magmas and/or contaminants in the province (>0.714; Innocenti et al., 1992; Conticelli, 1998; Dini et al., 2002) are not indicative of a metasedimentary, crustal melt as a mixing end-member as proposed for the Monte Capanne pluton (Giraud et al., 1986; Poli, 1992).

3. Analytical methods

Major elements (apart from Na_2O, MgO and FeO, which were determined by wet chemistry) were analysed by XRF at the University of Perugia, with full matrix corrections following Franzini and Leoni (1972). Cr, Sr, Ba, Zr and La were also analysed by XRF following Kaye (1965), with a precision better than 10% for Cr, Ba and Zr, and better than 5% for Sr and La. Accuracy was assessed using international standards and is better than 10% for most elements.

Whole-rock Sr isotopic analyses were performed at the Atlantic Universities Radiogenic Isotope Facility (Canada) on a Finnigan MAT 262V. Replicate analyses of SRM 987 standard yielded a $^{87}Sr/^{86}Sr$ value of 0.71025 ± 1 with an external reproducibility better than 2×10^{-5}.

Backscattered (BSE) imaging and chemical analyses of minerals were carried out using a JEOL 8900 RL electron microprobe (EPM) at the Department of Geochemistry, 'Geowissenschafliches Zentrum der Universitat Göttingen' (GZG). Accumulated BSE images on individual crystals were obtained after 20 scans using an acceleration voltage of 15 kV. A probe diameter of 5–10 μm, an accelerating voltage of 15 kV and a 20 nA current were used for quantitative plagioclase analyses. The counting time for the major element (Si, Na, K, Ca and Al) was 15 s on-peak, with backgrounds analysed for 5 s. Counting times for the minor elements (Fe, Sr) were 120 s on-peak and 60 s on backgrounds. Under these conditions, the detection limits were 55 ppm (Fe) and 100 ppm (Sr). Analytical errors were estimated from counting statistics for each analysis. Analysis of Ba was attempted, but the relatively low Ba contents of the Capraia plagioclases resulted in analyses either below detection limit (91 ppm), or of poor precision. Thus Ba has not been considered further in this study, although the low Ba content of the Capraia plagioclase phenocrysts compared to other examples is noteworthy (Singer et al., 1995; Ginibre et al., 2002). For pyroxene, Mn and Cr peaks were analysed for 30 and 60s respectively, with half of these times on the background, with detection limits of 91 ppm (Mn) and 122 ppm (Sr).

Microsampling for Sr isotopic analysis was performed using a Merchantek Micromill at the Institute for Geography and Geology, Copenhagen on plagioclase phenocrysts that had been previously imaged and analysed by electron microprobe. Plagioclase was drilled with a 0.5 mm diameter diamond-drill bit. The resulting microdrilled samples were selected to be sufficiently large (100–150 μm deep, 0.1–0.6 mm wide) to allow Pb isotopic analyses. The thin-sections were ultrasonically cleaned in dilute HCl prior to and after removal of each microdrill sample to avoid cross-contamination. The separation procedure for Sr is similar to that described in Charlier et al. (2006). Single use columns were made from polypropylene frit material and disposable 300 μl pipette tips (all pre-cleaned). Samples were loaded on fresh pre-cleaned Sr-Spec resin, and washed with alternating 3 M HNO_3, 0.05 M HNO_3 and 6 M HCl. The samples were washed in 3 M HNO_3, and Sr was collected in 0.05 M HNO_3. Samples were loaded with Ta activator on Ta or Re filaments and analysed in a VG Sector 54 thermal ionization mass spectrometer (TIMS) in multi-dynamic mode. Blanks including both sampling and chemical procedures were on average 40–50 pg, which is negligible considering the relatively large sample sizes (estimated > 0.01–0.1 mg), high Sr contents (>1000 ppm; Figs. 4, 5; Electronic Appendix) and similar blank and sample compositions (blank = $^{87}Sr/^{86}Sr \sim 0.71–0.72$). The NBS987 standard gave a mean $^{87}Sr/^{86}Sr$ value of 0.710235 ± 23 (2SD; n=4) during

the course of this study. In view of the low Rb/Sr ratios of the Capraia plagioclases (<0.01; measured by LA-ICPMS) and their young age (Fig. 1), measured $^{87}Sr/^{86}Sr$ can be considered to represent the initial isotopic ratios.

4. Samples

Plagioclase zonation was investigated in dacites from the early MC (samples MC50 and MC76; Fig. 1) and the late MR (samples MR20 and MR25; Fig. 1)

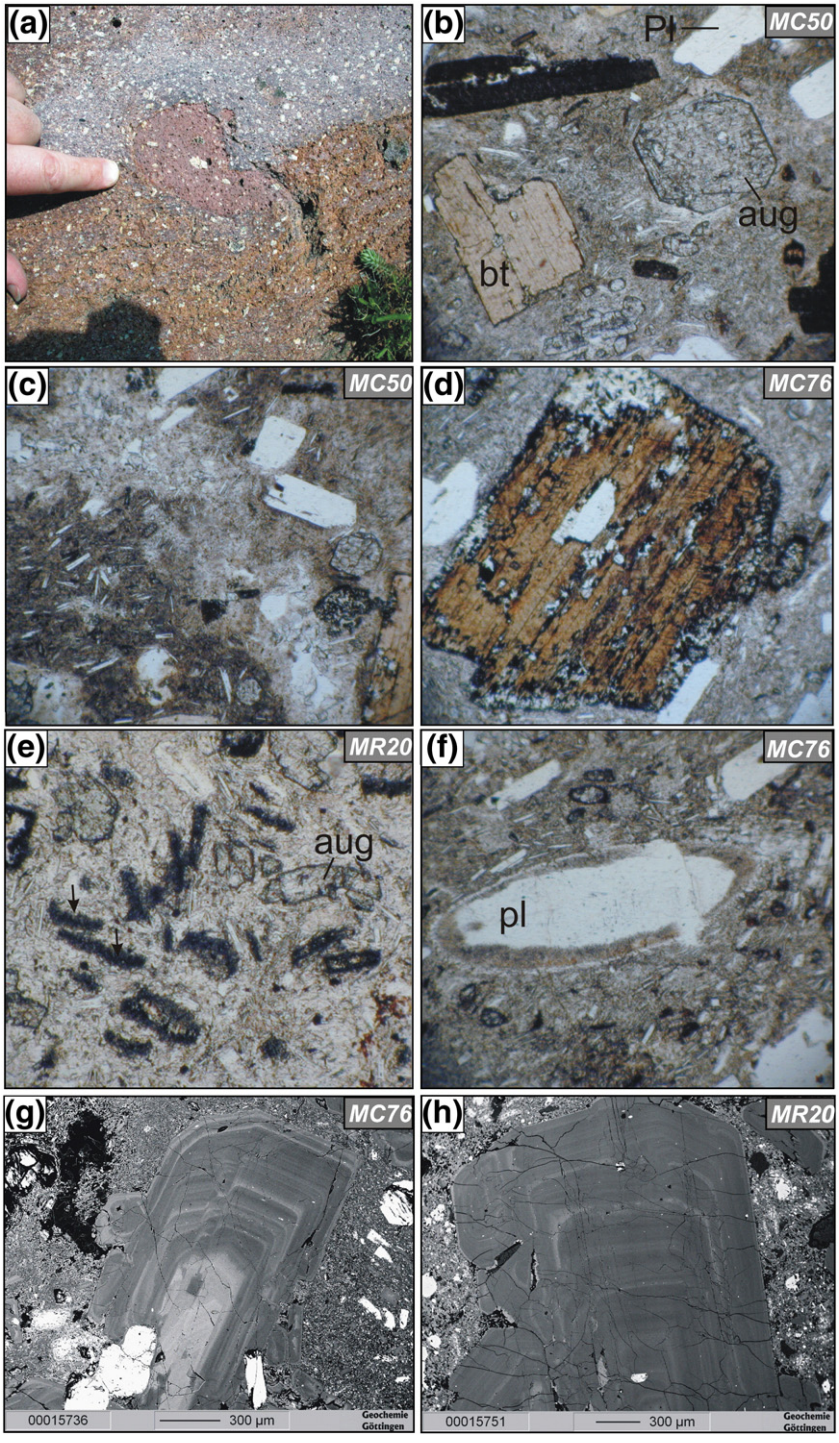

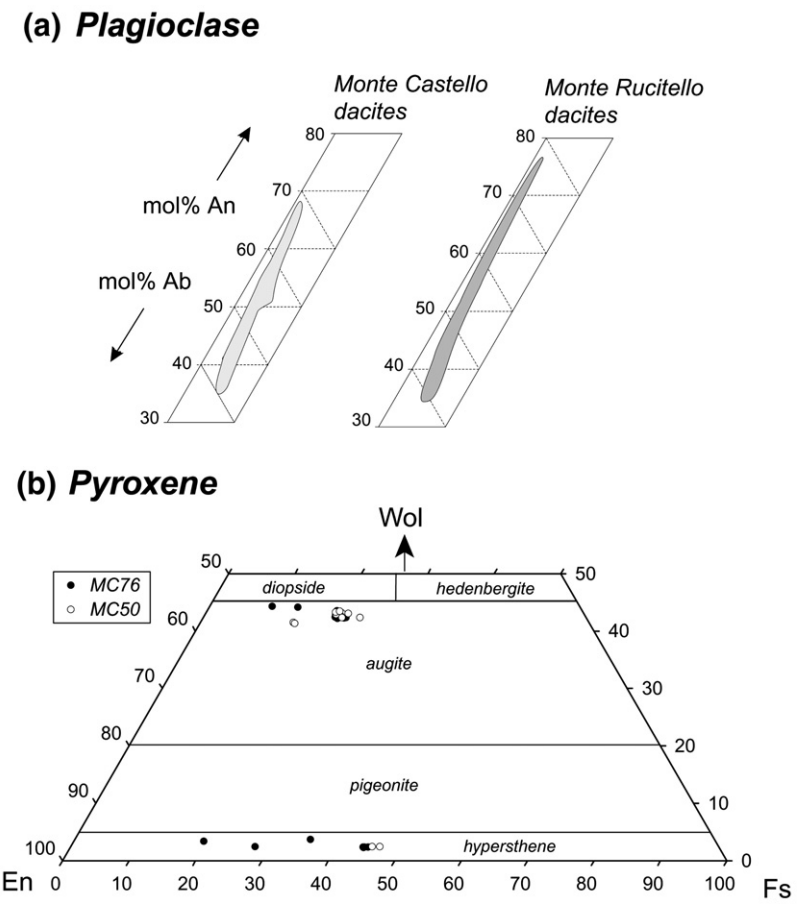

Fig. 3. Major element compositions of (a) plagioclase in the Monte Castello (MC) and Monte Rucitello (MR) and (b) pyroxene only in the MC dacites. The quadrilateral diagram for the classification of pyroxene is from Morimoto (1988).

units of the first eruptive cycle. We emphasise that these samples are not representative of the entire stratigraphy (Fig. 1) but display the best examples of plagioclase zoning. In order to assess the variability in plagioclase zoning within the largest MC unit, two representative samples from the north and south of the island were studied in detail (Fig. 1).

Pyroxene chemical data are also presented for two MC dacites (MC76 and MC50; Figs. 1 and 3; Table 3). The modal proportion of phenocrysts, as well as whole-rock major and trace element data for all samples are reported in Table 1. Major elements show a rather restricted range of compositions (SiO_2=62.2–63.0 wt.%; MgO=2.6–3.5 wt.%; CaO=4.3–4.9 wt.%) but a wider range of trace element contents (Sr=343–1184 ppm; Ba=688–1558 ppm) (Table 1).

5. Petrography

The petrography of the four samples investigated is typical of calc-alkaline magmas, with a high phenocryst content (>20%) consisting of plagioclase, clinopyroxene,

Fig. 2. (a) Field photograph of dacite from the Monte Campanile (MC) system (Fig. 1), illustrating compositional banding and (rare) mafic enclaves, both attesting to magma mixing. (b) to (f): Photomicrographs of typical dacitic textures in Capraia. Field of view is *c.* 1.3 mm. (b) Euhedral to subhedral biotite, augite and plagioclase phenocrysts in dacite MC50. (c) Occurrence of two groundmass types in dacite MC50. (d) Example of ragged texture in biotite phenocrysts (dacite MC76) indicative of reaction with the melt (dissolution along crystal edges and cleavages). (e) 'Ghost' biotites (see black arrows) in dacite MR20, suggestive of pervasive heating and prolonged crystal resorption. These are especially abundant in the MR dacites and are recognizable by their habit and/or hidden birefringence, although larger phenocrysts may have a similar extent of resorption to that in dacite MC76. (f) Plagioclase phenocrysts exhibiting a sieved texture in dacite MC76; note the fluidal texture exhibited by groundmass material. (g) and (h) BSE images of plagioclase phenocrysts from MC (g) and MR (h) dacites, respectively. Note that these two phenocrysts (*MC76-ph1* and *MR20-ph1*) were also analyzed by electron microprobe and TIMS (Figs. 4a, 5a and 7).

Table 1
Chemical composition, Sr isotopic composition and modal analyses of the four samples discussed in the text

sample	MC76	MC50	MR20	MR25
unit	M^{te} Castello	M^{te} Castello	M^{te} Rucitello	M^{te} Rucitello
SiO_2	63.34	62.03	63.52	62.20
TiO_2	0.77	0.97	0.67	0.67
Al_2O_3	15.79	16.54	15.46	16.00
Fe_2O_3	1.39	3.35	2.42	4.62
FeO	2.96	1.80	1.90	0.00
MnO	0.09	0.06	0.06	0.09
MgO	3.33	2.60	3.55	3.06
CaO	4.31	4.34	4.45	4.92
Na_2O	3.52	3.53	2.91	3.27
K_2O	3.23	3.71	3.89	3.95
P_2O_5	0.26	0.36	0.35	0.29
LOI	1.02	0.70	0.81	1.10
Total	100.01	99.99	99.99	100.17
Cr	89	94	95	100
Rb	182	187	147	164
Sr	494	498	1184	1110
Ba	688	828	1558	1220
La	60	68	150	127
Zr	238	259	215	204
$^{87}Sr/^{86}Sr_{(i)}$	0.70901	0.70951	0.70960	0.71021
2SE	0.00002	0.00001	0.00001	0.00003
Modal abundance of phenocrysts				
Olivine	–	1.8	–	–
Pyroxene	6.0	9.0	4.8	4.9
Amphibole	–		0.5	4.2
Biotite	7.6	9.7	7.2	5.2
Plagioclase	19.5	28.8	9.2	14.8
K-feldspar	–	–	0.1	–
Oxides	–	–	0.1	–
Total	33.1	49.3	21.9	29.1

orthopyroxene and biotite. The MC and MR units have similar mineralogy, but the occurrence of both amphibole micro-phenocrysts in dacite MR25 and olivine in dacite MC50 is noteworthy (Table 1). Moreover, the MC dacites are richer in phenocrysts (>30–40%) compared to MR (<30%) (Table 1). The groundmass consists of the same minerals, plagioclase being dominant, with Fe–Ti oxides in addition (Table 1) and sometimes shows a flow alignment (MC76; Fig. 2f). In dacites MC50 and MR25, two type of groundmass can co-exist (hypocrystalline and holocrystalline; Fig. 2c). Accessory minerals are ilmenite, zircon, titanite and apatite.

Plagioclase (<5 mm) is the most abundant phenocrystic phase in all lavas, but tends to be most abundant in MC lavas (Table 1), together with mm-size glomerocrysts of plagioclase, clino- and orthopyroxene and biotite. Plagioclase phenocrysts are zoned in most cases, exhibiting both short- and long-scale oscillations, interrupted by resorption events, defining variable oscillatory zoning (Fig. 2g,h). Irrespective of the type of oscillatory zoning, phenocrysts may display a sieved mantle (<100–150 μm; Fig. 2f). In the MR dacites, entire phenocrysts may exhibit a sieved (or dusty) texture.

Subhedral biotite phenocrysts (<1.5 mm) may have a ragged habit (Fig. 2d) with partial replacement by Fe–Ti oxides, but the extent of resorption is highly variable from one sample to another. Biotite may display a nearly pristine habit (dacite MC50; Fig. 2b) or be mildly (dacite MC76; Fig. 2d) or thoroughly (dacite MR20) resorbed. Biotite microcrysts may also appear as crystal 'ghosts' replaced by oxides and groundmass material (Fig. 2e), thus the original abundance of biotite (Table 1) may be underestimated.

Table 2
Selected plagioclase compositions in the Capraia lavas

Sample	MC76-ph1			MC76-ph2				MR20-ph1		MR25-ph1		
	Core	Inner rim	Outer rim	Core	Core	[DZ_4]	Outer rim	Core	Outer rim	Core	Interm	Outer rim
SiO_2	50.53	53.57	55.34	56.38	52.07	52.69	55.62	58.14	53.16	48.92	57.87	54.68
Al_2O_3	31.31	29.24	27.94	27.30	30.20	30.10	27.94	26.54	30.10	33.47	27.01	29.03
FeO	0.21	0.22	0.39	0.22	0.22	0.23	0.28	0.11	0.59	0.13	0.10	0.52
CaO	13.70	11.04	9.69	9.13	12.46	12.13	9.82	7.86	11.87	15.24	8.16	10.50
Na_2O	3.57	4.99	5.70	5.89	4.32	4.41	5.54	6.48	4.23	2.63	6.13	4.86
K_2O	0.24	0.39	0.50	0.65	0.33	0.33	0.46	0.62	0.30	0.15	0.65	0.33
SrO	0.21	0.15	0.16	0.15	0.16	0.15	0.14	0.16	0.23	0.14	0.17	0.20
wt-total	99.79	99.63	99.75	99.76	99.76	100.07	99.82	99.93	100.53	100.70	100.10	100.12
An	67.0	53.8	47.1	44.4	60.3	59.2	48.2	38.7	59.7	75.5	40.7	53.4
Ab	31.6	44.0	50.1	51.8	37.8	38.9	49.1	57.7	38.5	23.6	55.4	44.6
Or	1.4	2.3	2.9	3.8	1.9	1.9	2.7	3.7	1.8	0.9	3.8	2.0

Interm = intermediate; [DZ_4] = at dissolution zone 4 (see Fig. 4b).
MC76-ph1 and *MC76-ph2* phenocrysts are from the same thin-section.

Pyroxene phenocrysts are euhedral to subhedral (Figs. 2b, 6). Zoning is marked by concentric arrangements of apatite inclusions in augite crystals (Fig. 6a, b). Large augite phenocrysts may be mantled by olivine, itself surrounded by individual grains of hypersthene (sample MC76), while smaller augite crystals may be rimmed by a corona of diopsidic augite and subhedral apatite grains (Fig. 6d).

6. Mineral chemical zoning

6.1. Plagioclase

Six plagioclase phenocrysts from four dacites were chosen for further investigation following thin-section examination: four from the MC series (two each from MC76 — *MC76-ph1*, *MC76-ph2* and MC50 — *MC50-ph1* and *MC50-ph2*, both pairs from single thin-sections) and two from the later MR series (MR20 — *MR20-ph1* and MR25 — *MR25-ph1*). Representative plagioclase analyses are presented in Table 2, and the whole set of EMP data is found in the Electronic Appendix.

Both accumulated and single-scan BSE images together with mol% An, Sr and Fe zoning profiles for MC and MR plagioclases are presented in Figs. 4 and 5, respectively. Generally, each phenocryst records a complex differentiation history punctuated by multiple resorption events (RE). We define a resorption event as a sharp, or convoluted, compositional limit, and a dissolution zone (DZ) as a region where several RE occur close to one another (e.g., Tepley et al., 2000). We consider that these zones relate to a single chamber-wide magmatic event, producing An spikes associated with a series of major RE related to changes in an intensive parameter (P, T, X_{H2O}). Dissolution zones (DZ) may have a width of c. 100 μm (Figs. 4, 5), as well illustrated by plagioclase *MC76-ph2* (Fig. 4b). Growth zones range in size from c. 0.2 mm to 1.2 mm.

Because each phenocryst has its own morphology and zoning pattern, we treat each separately, prior to more general considerations. When describing the profiles, the core and rim regions have been arbitrarily fixed (with the distance in brackets).

6.1.1. Monte Castello (MC) dacites

Phenocryst *MC76-ph1* displays a high mol% An core terminated by a RE (Fig. 4a). Compared to the medial region (0.2–0.5 mm; Fig. 4a), where oscillations in the An content have large wavelengths and compositional zones are more diffuse, oscillations at the rim region (last 0.4 mm) are better defined and have smaller wavelengths (Fig. 4a). These are separated by abundant, closely-spaced oscillatory zones (max. 20 μm) separated by minor resorption events ("saw-tooth patterns"; Ginibre et al., 2002) with amplitudes of a maximum of 3 mol% An. Fe, however, displays little variation (1855±80 ppm) throughout the crystal, but concentrations tend to be higher in the core region than in the rim, apart from a distinct increase in the outer rim (up to 3540 ppm; Fig. 4a). Though Sr data are not as precise as Fe, a high Sr core is still distinguishable (Fig. 4a).

Phenocryst *MC76-ph2* is larger (1.9 mm) than *MC76-ph1* (1 mm) and is texturally more complex. Overall, the core (0–0.7 mm) exhibits fewer RE than the rim region (1.1–1.9 mm), but displays patchy zones (i.e., between 0.5–0.7 mm) and a resorbed core (Fig. 4b). Oscillatory zoning is well defined in the rim region, somewhat resembling textures found in *MC76-ph1* (Fig. 4b). Similarly, *MC76-ph2* also displays high mol% An in both core and rim, as well as limited Fe variations (1880±109 ppm), yet variations in the profile are detectable, and a pronounced increase of Fe in the outer rim (up to 2602 ppm) following a very convoluted RE is noteworthy (Fig. 4b).

Similar to other plagioclases in MC76, the wavelength of the oscillatory zoning in *MC50-ph1* decreases from core to rim (Fig. 4c). Low mol% An in the core and the rimward increase of Fe are noteworthy (Fig. 4c) and contrast with *MC76-ph1* and *MC76-ph2*. The rim region (outer 0.3 mm) consists of a highly convoluted RE, followed by a series of RE, sometimes cross-cutting each other (Fig. 4).

Phenocryst *MC50-ph2* has a complex, patchy-zoned core (Fig. 4d), whose high mol% An (67.5) outer rim grades towards lower An content and short wavelength oscillations, resembling the rim of plagioclase *MC50-ph1* (Fig. 4d). Moreover, similar to *MC50-ph1*, the rim grades towards high Fe (Fig. 4d).

6.1.2. MR dacites

Phenocrysts *MR25-ph1* and *MR20-ph1*, although larger (>2 mm), have textural features and chemical patterns (mean An content of 42.2±6.5 and 45.1±6.0 for the MR and MC plagioclases, respectively) that resemble the MC plagioclases (Fig. 5a, b). More specifically, *MR25-ph1* has both a small high-An core and several RE that are followed by distinctive decreases in the An content (Fig. 5b), although the true extent of resorption features may be underestimated due to the poorer resolution of the BSE image (only one BSE scan; Fig. 5a, b) compared to those of the MC plagioclases (Fig. 4). The mean Fe content of the MR plagioclases is distinctively lower (~35%) than the MC plagioclases, and, apart from the outer 1 mm in *MR25-ph1*, a general core-to-rim decrease is noteworthy (Fig. 5a, b). The outer rims of the MR plagioclases are also enriched in Sr, An, and Fe (Fig. 5a, b).

6.2. Pyroxene

Representative pyroxene analyses are presented in Table 3. The locations of the probe analyses together with the BSE images are shown in Fig. 6.

Both augite and hypersthene have variable compositions (Fig. 3b) that range parallel to the En–Fs join and there is no significant difference in pyroxene composition between the two MC samples (MC50 and MC76). Most grains in the MC dacites cluster in composition (Fig. 3b),

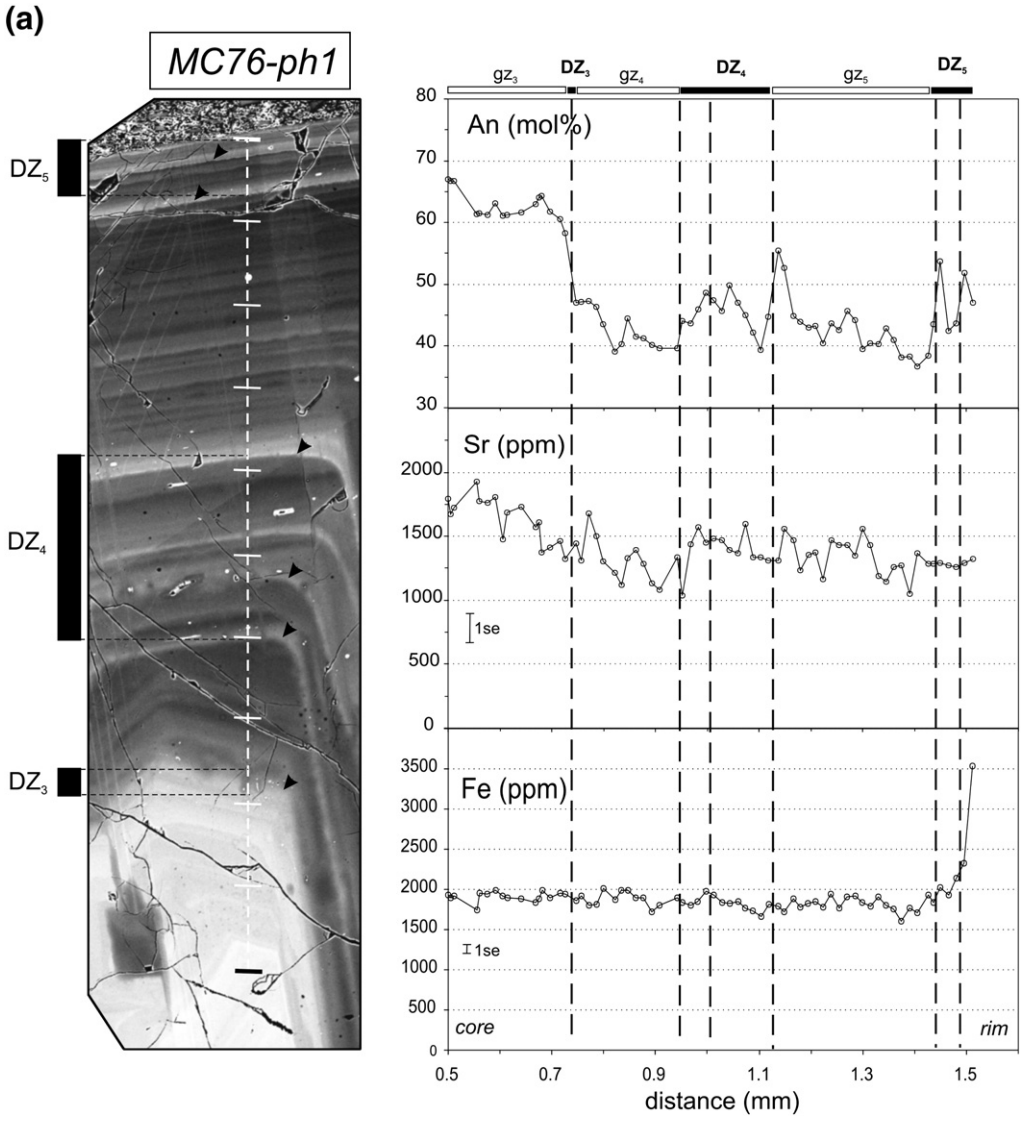

Fig. 4. Accumulated BSE images and An, Sr and Fe profiles (from EMPA data) in plagioclase phenocrysts from the Monte Rosso (MC) dacites. (a) *MC76-ph1*; (b) *MC76-ph2*; (c) *MC50-ph1* and (d) *MC50-ph2*. Abbreviations: gz = growth zone, DZ = dissolution zone. The dashed lines on the BSE image depict the electron microprobe traverses (with tick marks at 0.1 mm intervals) and the *x*-value corresponding to the profiles shown on the right hand side of the diagram. Note that the profiles for *MC76-ph1* and *MC76-ph2* do not start at zero. Their *x* datum (labeled on the BSE image) corresponds to the isotopic traverse presented in Fig. 7. The triangular markers indicate the main resorption events (RE), which are shown as dashed lines in the electron microprobe traverses beside the BSE images. Major RE are either indented or convoluted. These may be followed by newly-grown plagioclase with minute inclusions (apatite?) and also correspond to variable increases in mol% An. For the sake of clarity, minor resorption surfaces (as described in Ginibre et al., 2002) are not explicitly labelled in these figures, and can be best seen in (a), (c) and (d). The three data points in the core of *MC50-ph2* (Fig. 4d) fall outside the BSE image. Phenocryst *MC76-ph2* (b) has been taken as a normalizing reference for the other MC phenocrysts (=Ph_{ref}; see text). For *MC76-ph1* (a) and *MC50-ph2* (c), the rectangular back and white markers beside the BSE image indicate the dissolution zones (DZ) and the growth zones (gz), respectively, as defined in phenocryst *MC76-ph2* (b).

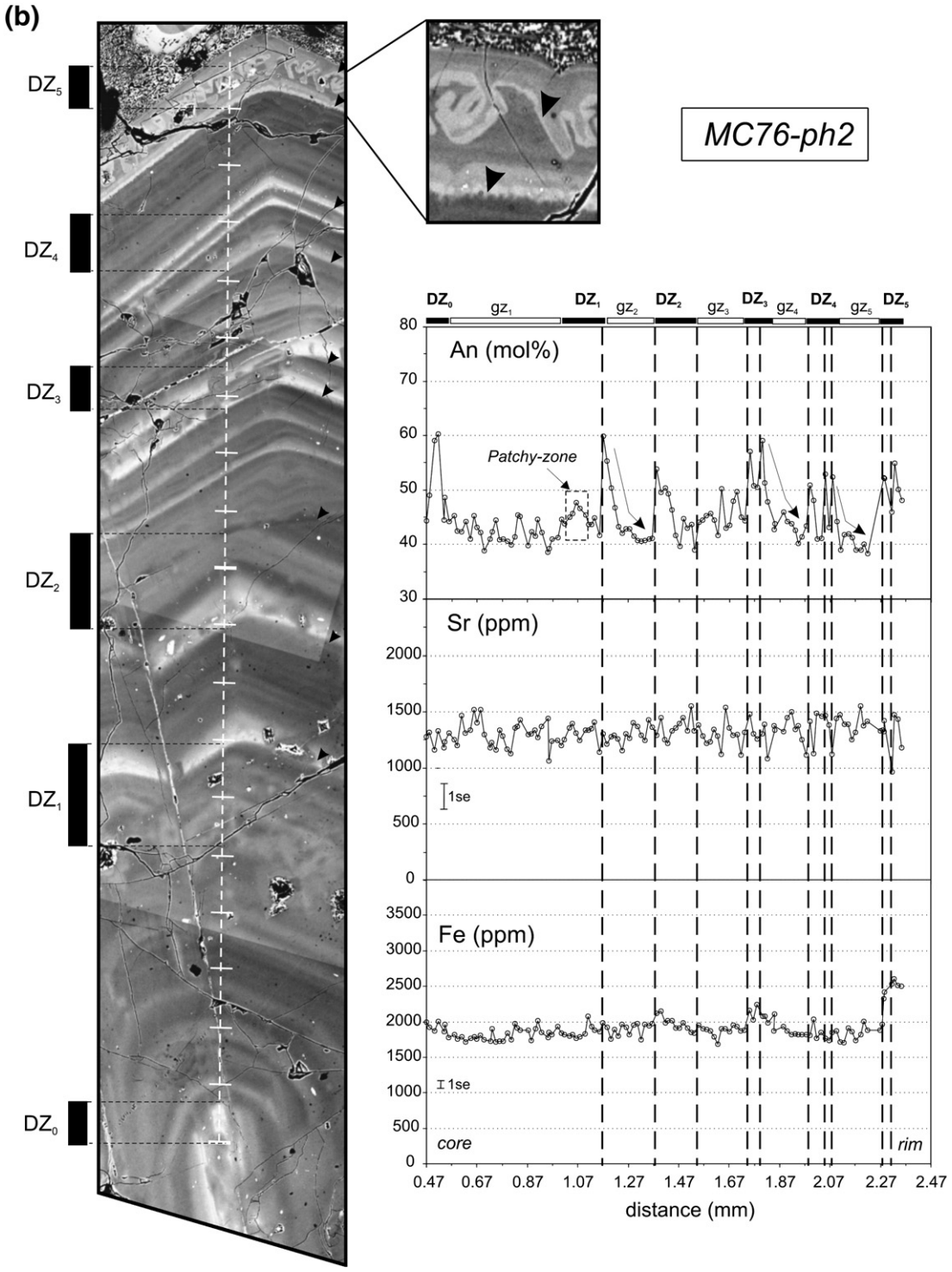

Fig. 4 (*continued*).

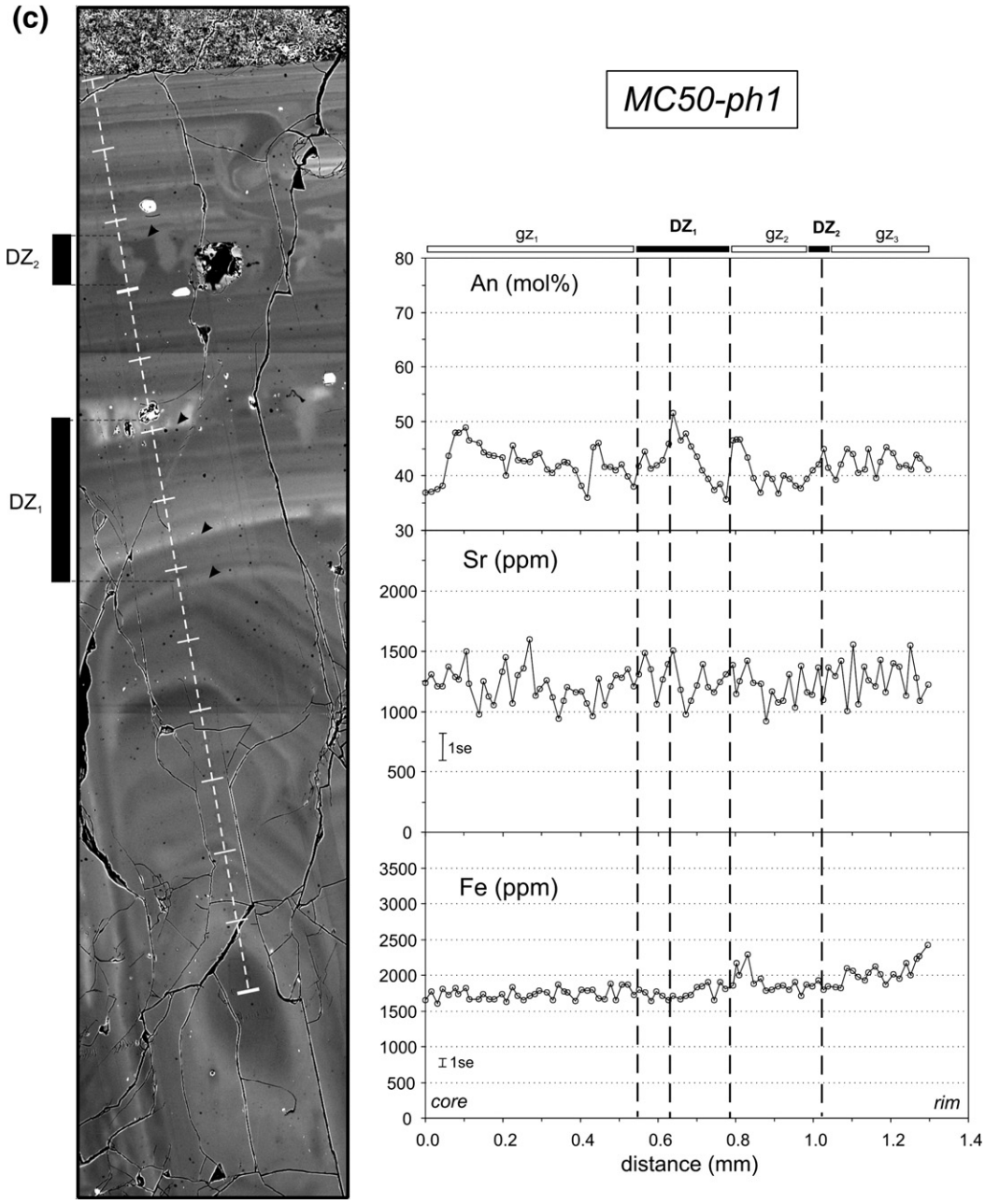

Fig. 4 (*continued*).

although the occurrence of grains with high Al_2O_3, TiO_2 and Mg-number is noteworthy (Fig. 3; Table 3). Augite and hypersthene both show insignificant variations in Wo content (maximum core-to-rim variations of 1–2%).

With the exception of one grain in dacite MC50 (Fig. 6d), augite displays weak reverse zoning (Mg-number increases by a maximum of 5) towards more magnesian compositions (Fig. 6). While reverse zoning seems to be predominant, augite crystals also exhibit weak normal zoning (from a Mg-number of 69 to 67) sometimes terminated by a Mg-rich rim, similar to that observed in hypersthene phenocrysts (Fig. 6a).

7. Mineral isotopic zoning

Most of the Sr isotopic analyses were obtained from two plagioclase phenocrysts from an MC dacite (*MC76-ph1* and *-ph2*) and one from an MR dacite (*MR20-ph1*).

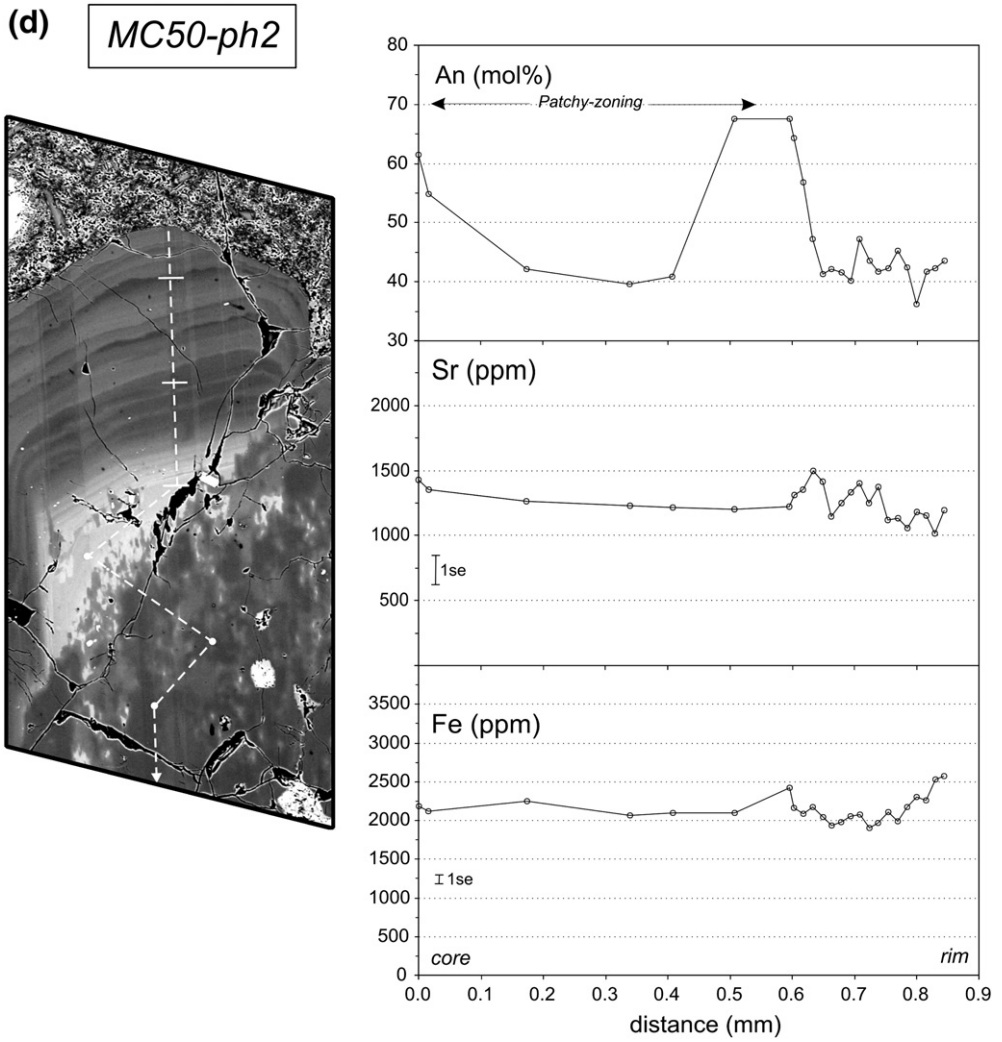

Fig. 4 (*continued*).

Isotopic analyses also include the cores of *MC50-ph2* and *MR25-ph1*, the rim of *MC50-ph1* as well as one clinopyroxene phenocryst in MC50. Results are summarised in Table 4 and the combined EMP-TIMS profiles for *MC76-ph1* and *-ph2* and *MR20-ph1* are shown in Fig. 7.

In general, the grains exhibit a wide range of $^{87}Sr/^{86}Sr$ (0.70872–0.71004) reminiscent of the range observed in whole-rock data from the entire complex ($^{87}Sr/^{86}Sr_i$=0.70727–0.71020; Poli and Conticelli, unpublished data), but larger than that observed in the host whole-rocks ($^{87}Sr/^{86}Sr_i$=0.70951–0.71021). Variations in $^{87}Sr/^{86}Sr$ along core-rim profiles also correspond to chemical variations (mol% An, Sr), and the occurrence of dissolution zones (Fig. 7). However, it is important to note that the sampling was designed with Pb isotopic analysis in mind, requiring larger samples than Sr, and hence less than optimal spatial resolution. Thus, our microdrilled samples may represent a mixture of zones of different isotopic compositions.

Most of the analysed cores from both units (apart from *MC76-ph1*) have a rather restricted range of $^{87}Sr/^{86}Sr$ (0.70971–0.71004). The core of *MC76-ph1* has significantly lower $^{87}Sr/^{86}Sr$ than the cores of the other crystals (Fig. 7a), becomes even less radiogenic rimwards before returning to a more radiogenic composition at its rim. *MC76-ph2* has a relatively homogeneous isotopic composition apart from a rimward increase in $^{87}Sr/^{86}Sr$ near its core and a distinctive decrease at the rim (Fig. 7b). The highly radiogenic $^{87}Sr/^{86}Sr$ at the rim of *MR20-ph1* is noteworthy (Fig. 7c; Table 4). In order to check the symmetry of the zoning patterns, we have analysed the core

and the rim on the other side of phenocryst *MR20-ph1*. Results (Table 4) show that the core ($^{87}Sr/^{86}Sr=0.70985$) is less radiogenic than the rim ($^{87}Sr/^{86}Sr=0.71000$), in perfect agreement with the more detailed traverse shown in Fig. 7.

8. Magmatic temperature estimates

Despite variable pyroxene composition (Figs. 3, 6) and the inherent difficulty of finding minerals in chemical equilibrium, an attempt was made to constrain magmatic temperatures using the pyroxene thermometer (based on experimentally-determined phase equilibria for Ca–Fe–Mg pyroxenes; Lindsley, 1983) with the aid of the QUILF software (Andersen et al., 1993). Textural context is critical for reliable temperature estimates. For example, we based our estimation for the MC dacites on a hypersthene (Wo_3 En_{52} Fs_{45}) inclusion enclosed in the core of an augite phenocryst (Wo_{43} En_{37} Fs_{20}); see Fig. 6c for location of the spots) in MC50, and two grains of

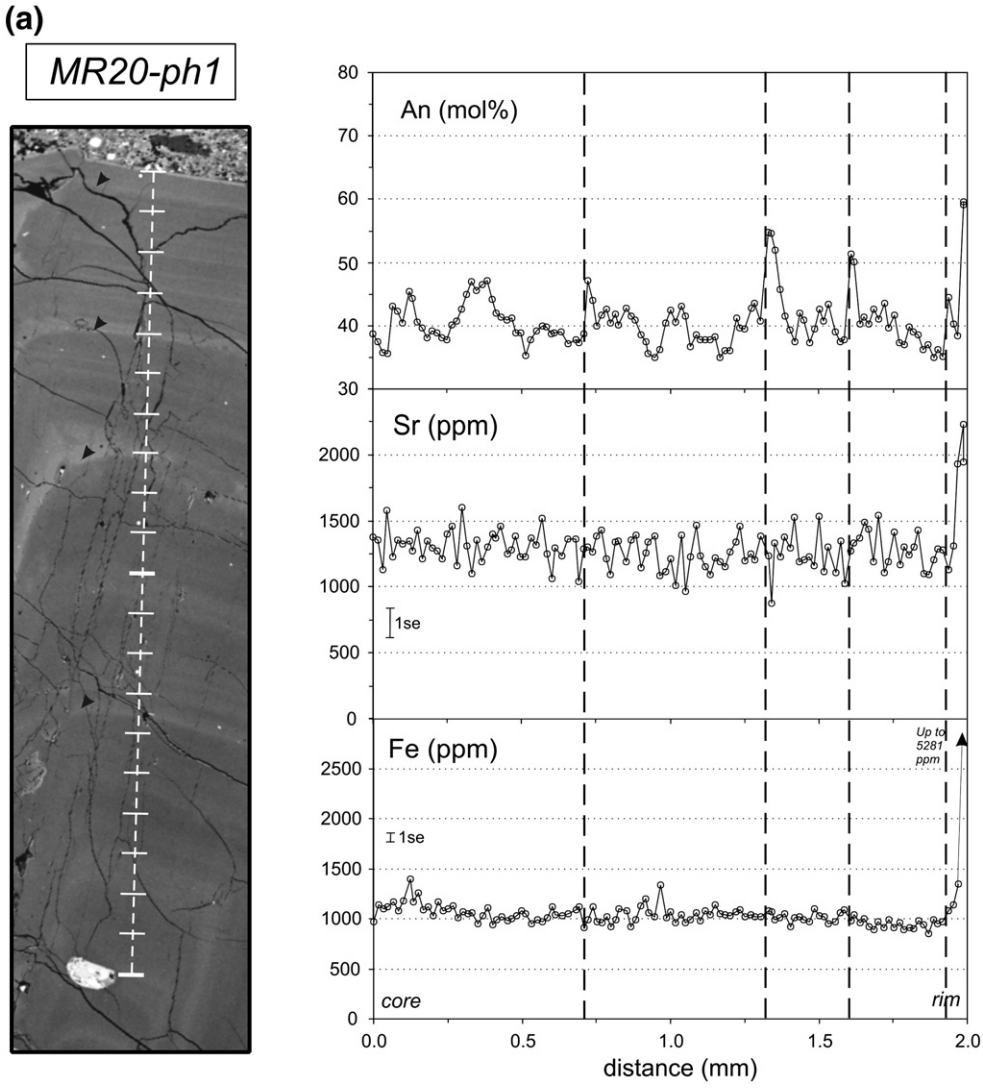

Fig. 5. Accumulated BSE images and An, Sr and Fe profiles in plagioclase phenocrysts from the Monte Rucitello (MR) dacites. (a) *MR20-ph1* and (b) *MR25-ph1,* ornamented and labelled as in Fig. 4. Arrows along the An profile in b)underline the decrease in An content after most resorption events, which are indicative of crystal fractionation after magma recharge episodes. Due to the lower resolution of these BSE images (single scan), growth and dissolution zones are less clearly distinguishable than in the MC plagioclases. Moreover, since there is no clear correlation with the MC plagioclase profiles, growth and dissolution zones have not been labeled. As a result, the true extent of resorption in the MR phenocrysts is probably underestimated.

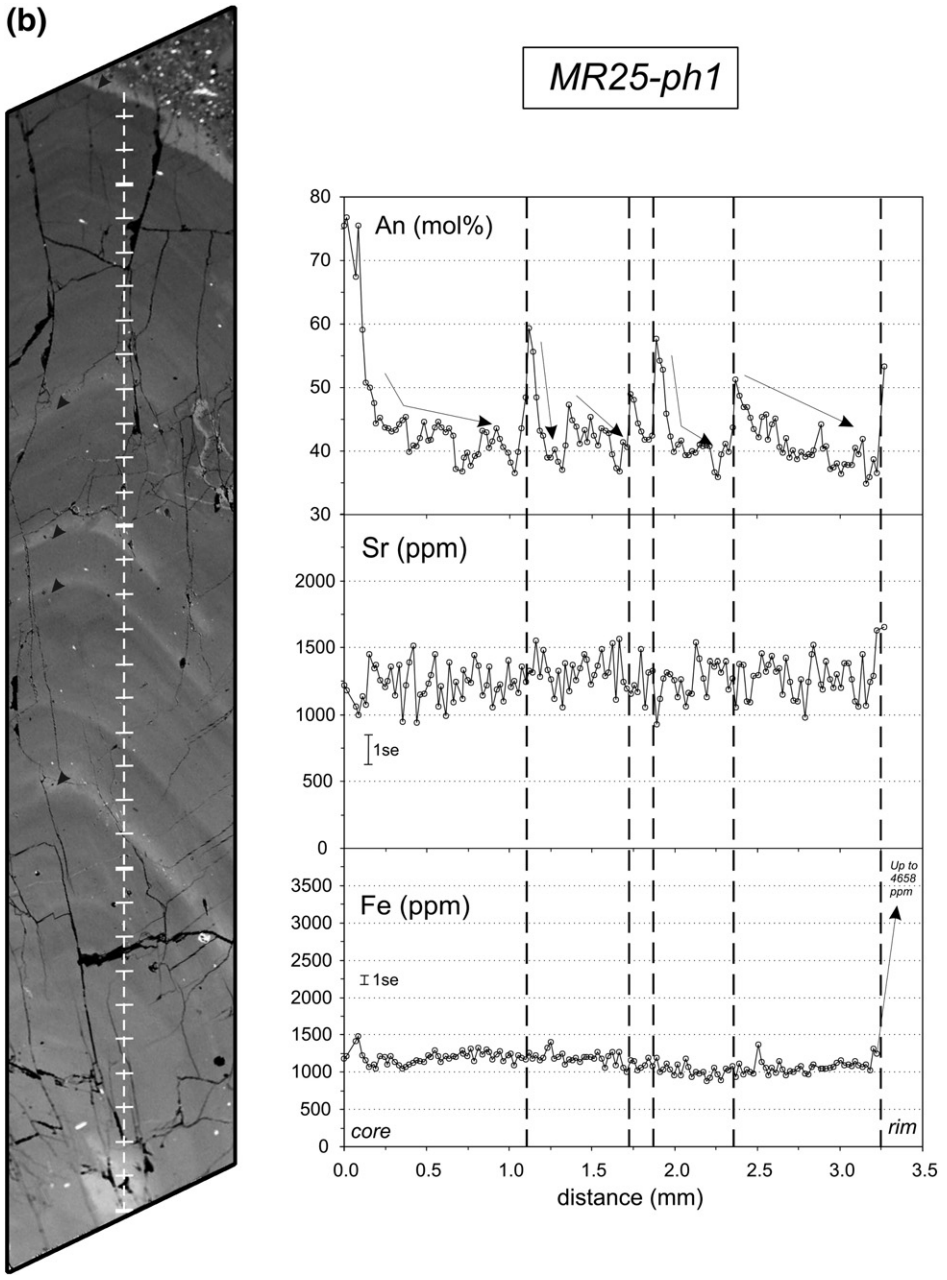

Fig. 5 (*continued*).

hypersthene (Wo_{02} En_{54} Fs_{44}) and augite (Wo_{43} En_{37} Fs_{20}) in contact with each other in MC76. Calculated temperatures (at a hypothetical pressure of 5 kbar) differ by *c.* 115 °C between hypersthene (790 ± 50 °C) and augite (675 ± 50 °C) for MC50 and MC76 samples, which is indicative of marked chemical disequilibrium between the two grains. These temperatures are thus not considered reliable.

Magmatic temperatures have also been assessed using zircon (Watson and Harrison, 1983) and apatite (Harrison and Watson, 1984) solubility equations. Zircon saturation temperatures range from 782–784 °C for the MC dacites and 759–779 °C for the MR dacites, i.e., consistent with the upper temperature range obtained using the two-pyroxene thermometer for the MC dacites. Apatite saturation temperatures are higher (i.e. >900 °C) than zircon saturation temperatures for both the MR and MC dacites. This discrepancy is not uncommon, and may be explained either by limitations to the model when

Table 3
Selected pyroxene analyses in the Capraia lavas

Sample	MC76			MC50			
mineral	hyp	hyp	aug	aug	aug	aug	aug
	core	rim	core	core	rim	core	rim
SiO_2	53.56	54.72	51.95	52.23	50.26	51.80	51.98
TiO_2	0.18	0.24	0.16	0.13	1.23	0.13	0.15
Al_2O_3	0.97	1.31	0.62	0.51	3.67	0.59	0.78
Cr_2O_3	0.29	0.09	–	–	0.04	–	0.03
FeO	17.84	12.65	12.99	11.67	8.32	14.03	12.46
MnO	0.31	0.27	0.49	0.46	0.22	0.56	0.52
MgO	25.50	28.53	12.71	13.03	15.20	11.79	12.78
CaO	1.23	1.73	20.72	21.03	19.70	20.44	20.50
Na_2O	0.01	0.03	0.22	0.21	0.27	0.24	0.26
K_2O	0.02	0.02	0.00	0.00	0.01	0.01	0.00
Total	99.90	99.59	99.86	99.28	98.93	99.60	99.45
Wo	2.4	3.4	42.0	42.9	41.0	42.0	41.9
En	69.8	77.0	35.9	37.0	44.1	33.7	36.4
Fs	27.8	19.5	21.3	19.3	13.9	23.4	20.7
Ac	0.0	0.1	0.8	0.8	1.0	0.9	1.0
Mg-number	73	81	66	68	79	62	67

aug = augite; hyp = hyperstene; interm = intermediate.

applied to aluminous compositions (Hoskin et al., 2000) or magma mixing (Gagnevin et al., 2004).

9. Element partitioning

Equilibrium Sr crystal-melt partitioning in plagioclase is primarily controlled by chemical composition (An content) and temperature, although variations in temperature have a secondary effect compared to crystal-chemical control (Blundy and Wood, 1991; Blundy and Shimizu, 1991; Ginibre et al., 2002). Fe in plagioclase is predominantly incorporated in the trivalent state (Smith and Brown, 1988), except in highly reducing conditions (Hattori and Sato, 1996). Thus, Fe partitioning is considered to be largely dependent on the redox state of the melt (fO_2; Wilke and Behrens, 1999), i.e. $D\mathrm{Fe}_{\text{pl-melt}}$ is high (0.55) under oxidising conditions and low (0.08) under reducing conditions (in tonalitic melts; Wilke and Behrens, 1999). However, $D\mathrm{Fe}_{\text{pl-melt}}$ may also depend on the bulk composition of the melt (i.e., SiO_2 content, relative proportion of FeO and Fe_2O_3; Lundgaard and Tegner, 2004), as well as the temperature (Longhi et al., 1976; Ginibre et al., 2002).

Excluding the rims, Fe does not display any obvious correlation with either An (not shown) nor $\mathrm{Sr}_{\text{melt}}$ (calculated using the equation RT ln D_{Sr}=26.8 – 26.7 * X_{An}, Blundy and Wood, 1991) in the Capraia plagioclases (Fig. 8b), supporting the assertion that the oxygen fugacity is likely the main control on DFe (e.g., Wilke and Behrens, 1999). However, although most of the data are clustered between *c.* 1600–2000 ppm Fe and 200–400 ppm $\mathrm{Sr}_{\text{melt}}$ (Fig. 8b), two trends can be distinguished, suggesting that changes in fO_2 were likely to have been accompanied by chemical variations in the ambient melt (i.e., Lundgaard and Tegner, 2004). Since K variations in plagioclase mirror temperature variations in the magma (Hattori and Sato, 1996), the crude correlation between Fe and K (not shown) further suggests that Fe partitioning in plagioclase is also, in part, temperature dependent (i.e., Longhi et al., 1976). Thus, partitioning of Fe is more ambiguous than Sr due to a combination of factors that may affect it. Changes in Fe content may reflect changes in oxygen fugacity, chemistry and temperature, which is consistent with magma mixing.

10. Evolution of the Capraia magma system

10.1. Petrographic and geochemical evidence for magma mixing.

Mixing of magmas is a process governed by chaotic dynamics (Perugini and Poli, 2000) and involves repetitive transfer of phenocrysts from one magma to another, resulting in a wide variety of disequilibrium textures (Blundy and Shimizu, 1991; Stimac and Pearce, 1992; Clynne, 1999; Tepley et al., 1999; Murphy et al., 2000; Couch et al., 2001; Troll and Schmincke, 2002; Perugini et al., 2003). In Capraia, mixing resulted in sieve-texture and patchy-zoning in plagioclase, Fe–Ti oxide pseudomorphs after biotite (Fig. 2) and reaction rims on pyroxene. Both biotite and plagioclase exhibit pristine and resorbed habits on the scale of the thin-section (Fig. 2). In particular, the pronounced dissolution in the MR dacite biotites (Fig. 2e) is consistent with input of a hot magma prior to eruption. Interaction between a dacitic and a more mafic component also occurred in the MC dacites, as indicated by high *mg*-number (>75) in the rim of some pyroxene phenocrysts (Fig. 6a, d) and the occurrence of olivine, either as xenocrysts (MC50), or as a reaction rim (Fo_{83}) replacing augite in a cpx–ol–opx composite grain (MC76; see above). The ol–opx transition in the composite grain suggests interaction with a more differentiated, andesite-like magma (Clynne, 1999; Coombs and Gardner, 2004).

The large compositional spread in both pyroxene and plagioclase phenocrysts (Fig. 3), variable trace elements (e.g., Sr=877–2232 ppm), major element contents (An=35–77 mol%) and Sr isotopic ratios ($^{87}Sr/^{86}Sr$=0.70872–0.71004) in plagioclase support a protracted open-system history (e.g., Feldstein et al., 1994; Feeley and Dungan, 1996; Tepley et al., 1999). Chemical and isotopic heterogeneities at the mineral-

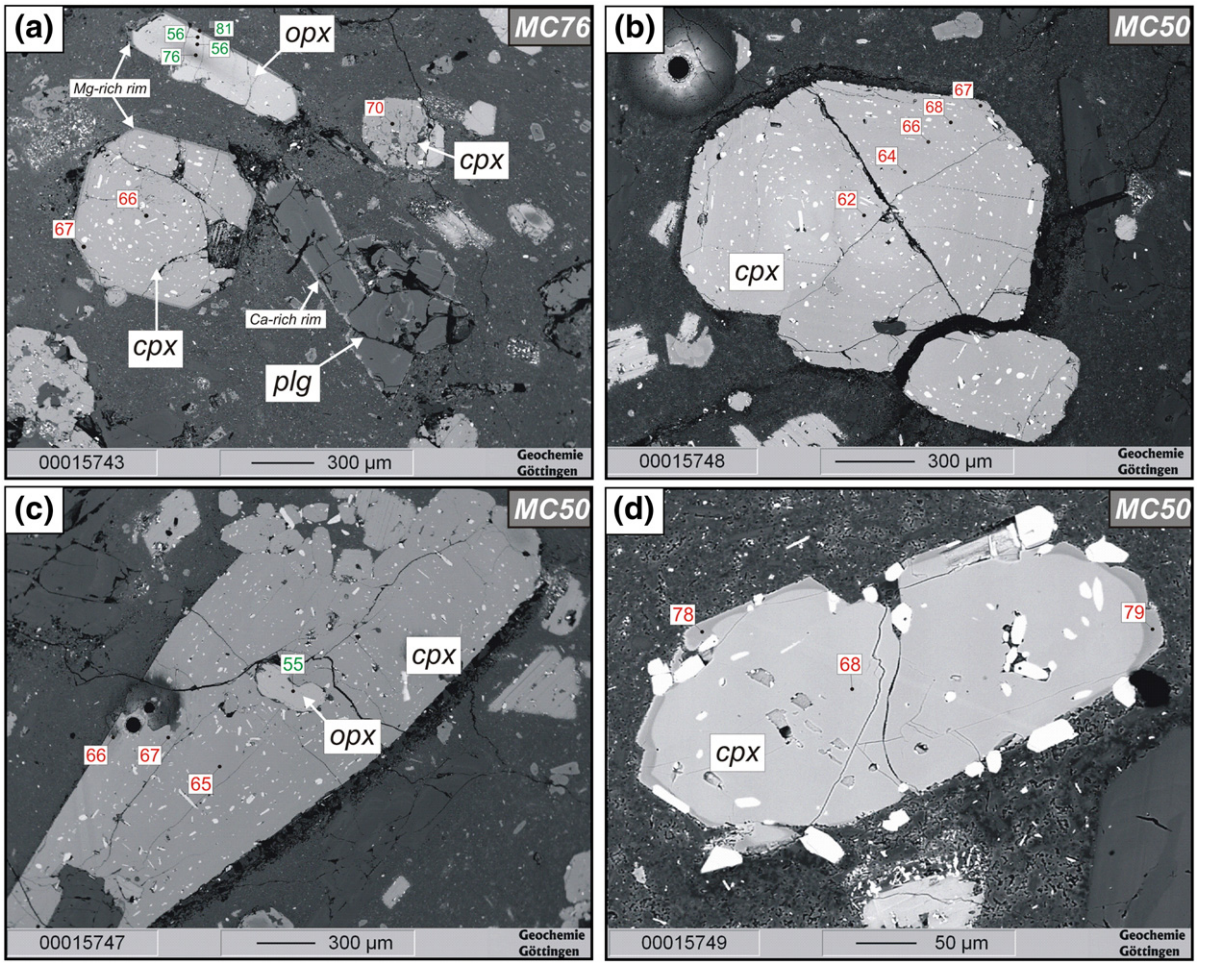

Fig. 6. BSE images and chemical zoning of pyroxene phenocrysts in the MC dacites. The numbers in the white boxes represent the Mg-number. The bright inclusions in most augite grains are apatite crystals, sometimes arranged crystallographically. White crystals in (d) are opaques. Note the occasional (often weak) reverse zoning for both augite and hypersthene phenocrysts, as well as the resorption event at the rim of the augite microphenocryst displayed in (d). One cpx–opx pair used for thermometric calculations is shown in (c).

scale result in large variations in trace element compositions (Ba, Sr and La) and $^{87}Sr/^{86}Sr$ (0.70862–0.71021; Table 1) on the whole-rock scale. More specifically, the MR dacites are strongly enriched in Ba, Sr and La and have generally more radiogenic Sr than the MC dacites (Table 1).

10.2. Chemical correlation between plagioclase phenocrysts

Through numerical simulations, Perugini et al. (2005) considered the effect of magma dynamics on the nature of oscillatory zoning in Capraia plagioclase phenocrysts, showing that (1) plagioclase growth occurred in a chaotic magma system and (2) oscillatory zoning can be accounted for by variable mixing depending on flow fields and amounts of nutrients for given 'attractors' (Perugini et al., 2005). However, these authors purposely did not take into account major resorption features in their modelling of oscillatory zoning in plagioclase. In their model, dissimilar zoning patterns are expected for a given time series and, as a consequence, correlations between intervals of plagioclase growth and evolution of the magmatic system would not be predicted. This contrasts with the view that, in the light of robust statistical methods (e.g., use of numerically generated profiles), phenocrysts may reveal 'shared histories' in their zonation patterns, giving further insight into their petrogenesis (e.g., Wallace and Bergantz, 2004, 2005).

Plagioclase phenocrysts in Capraia have complex textures consisting of different compositional zones separated by resorption events that are interpreted to have

Table 4
Sr isotopic composition of microdrilled plagioclase and clinopyroxene from Capraia Volcano

Sample No		$^{87}Sr/^{86}Sr$	2SE
MC76-ph1	Core	0.709192	0.000051
	|	0.708717	0.000041
	Rim	0.709545	0.000043
MC76-ph2	Core	0.709710	0.000068
	|	0.709878	0.000065
	|	0.709921	0.000040
	|	0.709825	0.000030
	|	0.709815	0.000018
	Rim	0.709448	0.000044
MC50-ph2	Core [a]	0.710017	0.000024
	Core [a]	0.709787	0.000037
MC50-ph1	Rim	0.709749	0.000037
MC50-cpx		0.709949	0.000028
MR20-ph1	Core	0.709786	0.000072
	|	0.709922	0.000041
	|	0.709929	0.000037
	Rim	0.710043	0.000048
	Core [b]	0.709853	0.000071
	Rim [b]	0.710004	0.000034
MR25-ph1	Core region	0.709830	0.000024
	Core region	0.709730	0.000023

$^{87}Sr/^{86}Sr$ is the measured ratio (no age correction due to low Rb/Sr ratio).
[a] Analyses in patchy core.
[b] Analyses from the other side of the same phenocryst.

formed in response to heating events (e.g. Tsuchiyama, 1985), suggesting repeated undercooling and disequilibrium conditions during crystal growth. Crystal resorption can be accompanied by nucleation of new crystals in equilibrium with the P–T–X_{H2O} conditions that prevail in the new magmatic environment.

We attempted to chemically correlate the plagioclase phenocrysts in the dominant MC dacitic unit, taking into account the position of the dissolution zones and the chemical response (using mol% An, Sr, Fe) after resorption. The method consists of 'stretching' and visually comparing the An profile with respect to a fixed, reference profile (*MC76-ph2* = Ph_{ref}) taking into account the width of the growth and dissolution zones (Fig. 9); Fe (minor element with the smallest error, i.e. SD < 5%) was then adjusted to the new Ph_{ref}-normalised distance (Fig. 9). We acknowledge that such correlations may be hazardous since the true cores of the crystals were not necessarily sampled and because crystals may not have been cut along common crystallographic orientations. However, our approach is not to compare crystal zoning on a short, micrometer-scale (cf. Wallace and Bergantz, 2004), because the chaotic nature of the interaction process (Perugini et al., 2003, 2005) would not permit such detailed comparison, but rather, through both plagioclase chemical and textural data, we want to test whether phenocryst growth can be correlated in the MC dacites.

Results show that the MC plagioclase phenocrysts can be correlated with one another on chemical grounds (Fig. 9). Plagioclase *MC50-ph1* records a similar chemical signature to the early stage of Ph_{ref} growth, i.e. consisting of a U-shape mol% An profile and a general core-to-rim increase in Fe ([gz1]; Fig. 9). Similarly, both Fe and mol% An profiles in *MC76-ph1* indicate that nucleation of the latter may correspond to a later stage of growth in *MC76-ph2* (([gz4] to [gz5]; Fig. 9), which is in agreement with the similar textures at these zones, i.e., short wavelength of the oscillatory zoning, abundant resorption events and complex texture at [DZ_5] (Fig. 4a, b). The validity of this model, with particular reference to the two phenocrysts in MC76 that were examined in detail, is discussed in the next section in the light of intra-grain variations in Sr isotopic composition. We find that the Sr isotopic compositions are not easily correlated between presumably co-existing phenocrysts, requiring complex magma-chamber dynamics.

10.3. Discussion

While mol% An cyclic variations associated with fine resorption surfaces reflect crystal motion along thermal and compositional gradients in a magma chamber ('convective crystal dispersion'; Ginibre et al., 2002), major dissolution surfaces with abrupt changes in the An content (>10%), sometimes associated with changes in isotopic ratio, are related to influx of magma and heating during recharge (Singer et al., 1995; Davidson and Tepley, 1997). In the case of the Capraia plagioclase, textural and chemical changes following dissolution zones indicate that such events may have occurred repeatedly in the Capraia magma system. The large size of most phenocrysts together with variation in Sr isotopic compositions and multiple resorption events are consistent with growth in a crystal-rich boundary layer close to the wall-zone of the chamber (e.g., Nakada et al., 1994). Magma recharge would have the effect of disrupting and admixing crystals from such a boundary layer into the surrounding convective magma (e.g., Davidson et al., 2001).

In the next paragraphs, we present our interpretative model for growth/resorption of the MR and MC plagioclases in the light of both chemical and Sr isotopic

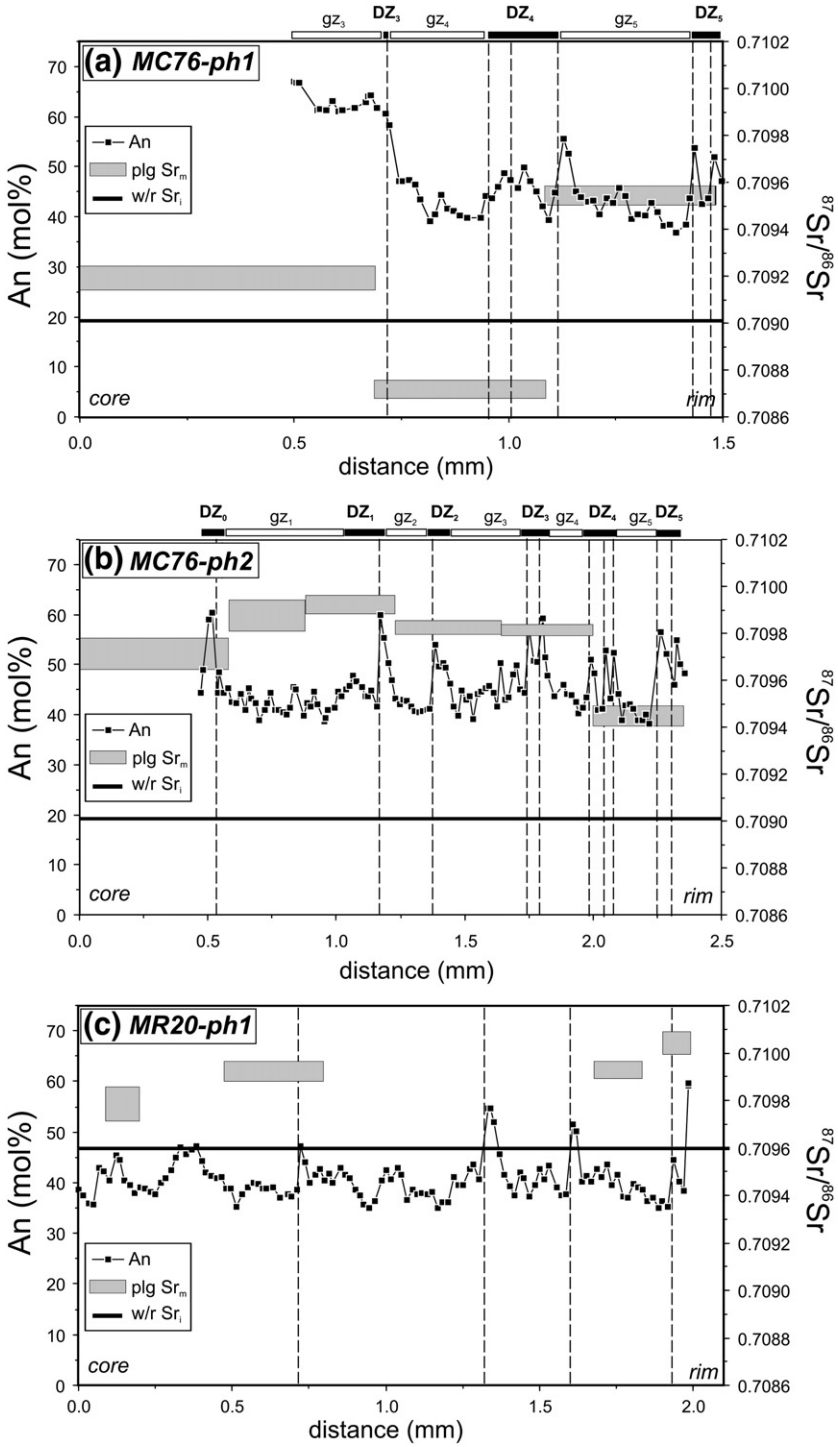

Fig. 7. Coupled $^{87}Sr/^{86}Sr$ - mol% An profiles for (a) *MC76-ph1*, (b) *MC76-ph2* and (c) *MR20-ph1*. See Fig. 4a, b for the labels of dissolution zones (DZ) and growth zones (gz). Size of the boxes for the $^{87}Sr/^{86}Sr$ data is proportional to the two-sigma error of the analysis and approximate sample area. Note that there are no isotope data from the middle of the traverse in *MR20-ph1* are due to failed analyses or analyses with unacceptably large errors (2SE > 100 ppm).

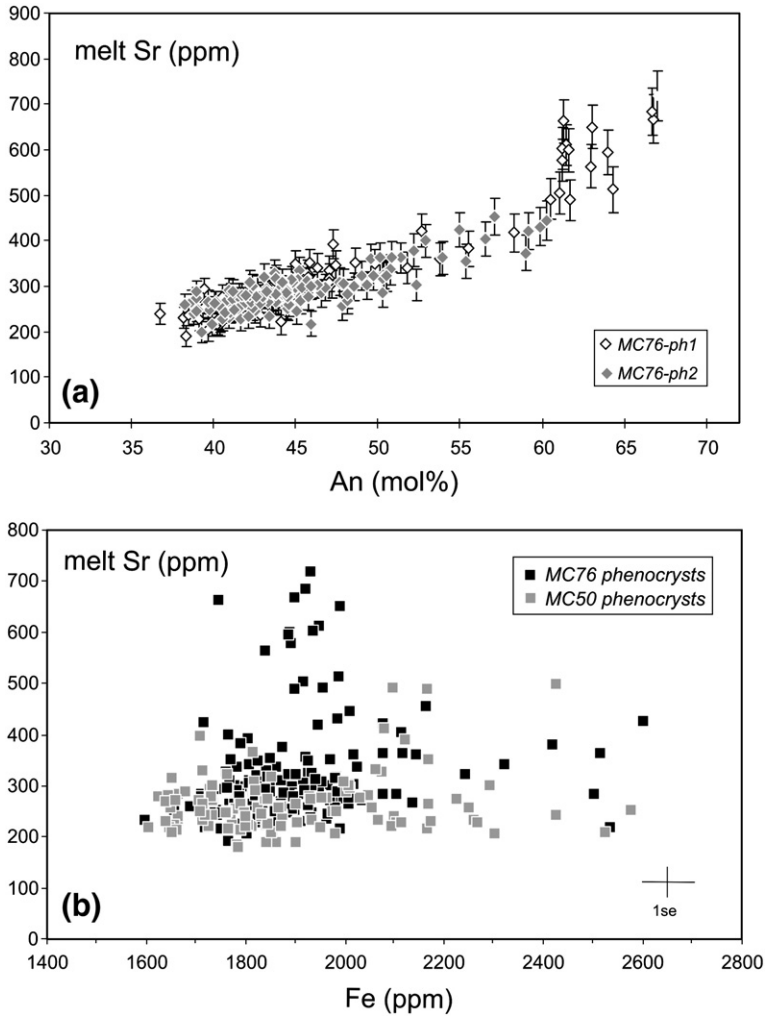

Fig. 8. Calculated Sr concentration in the melt (after Blundy and Wood, 1991) compared with (a) mol% An and (b) Fe in plagioclase phenocrysts from the MC dacites. Error bars for Sr_{melt} represent the analytical uncertainty for the electron microprobe Sr measurements (15–30%). While the former diagram illustrates magma mixing as a dominant process in the genesis of the MC dacites (using both phenocrysts in MC76 as proxies), domains in the Fe–Sr_{melt} diagram indicate that different fO_2 during growth was likely to be accompanied by changes in melt composition due to mixing.

data. In particular, we are testing the view that the MC phenocrysts have experienced common growth/dissolution cycles during differentiation (Fig. 9).

Using the chemical correlation framework developed above (Fig. 9), it is clear that the Sr isotopic compositions of phenocrysts *MC76-ph1* and *MC76-ph2* do not correlate simply with each other. While $^{87}Sr/^{86}Sr$ in *MC76-ph2* remains nearly constant along growth zones [gz_1] to [gz_4], $^{87}Sr/^{86}Sr$ in *MC76-ph1* has less radiogenic values – similar to the whole-rock value (Fig. 7a, b) – in growth zones [gz_3] and [gz_4] (Fig. 10). However, the rim region in both phenocrysts (at/after [DZ_4]), which exhibits fine-scale oscillatory zoning (Fig. 4a, b), displays a restricted range of Sr isotopic composition ($^{87}Sr/^{86}Sr$=0.70945–0.70955; Fig. 10). This is interpreted to represent a mixture between radiogenic (similar to the core of *MC76-ph2*) and unradiogenic (similar to the core of *MC76-ph1*) components. Recharge with unradiogenic magma is also suggested by the fact that the rim region in both crystals has lower $^{87}Sr/^{86}Sr$ than the whole-rock. This unradiogenic component may reside in the groundmass, which shows field and petrographic evidence for being heterogeneous, and makes up to 60% of the dacites (Table 1).

It is possible that *MC76-ph1* was a foreign, wall rock xenocrystic crystal and/or crystallized at a much earlier stage of differentiation (i.e., the dissolution event [DZ_4] removed a significant amount of the crystal) in order to account for the difference in isotopic composition between *MC76-ph1* and *MC76-ph2* from [gz_3] to [gz_4].

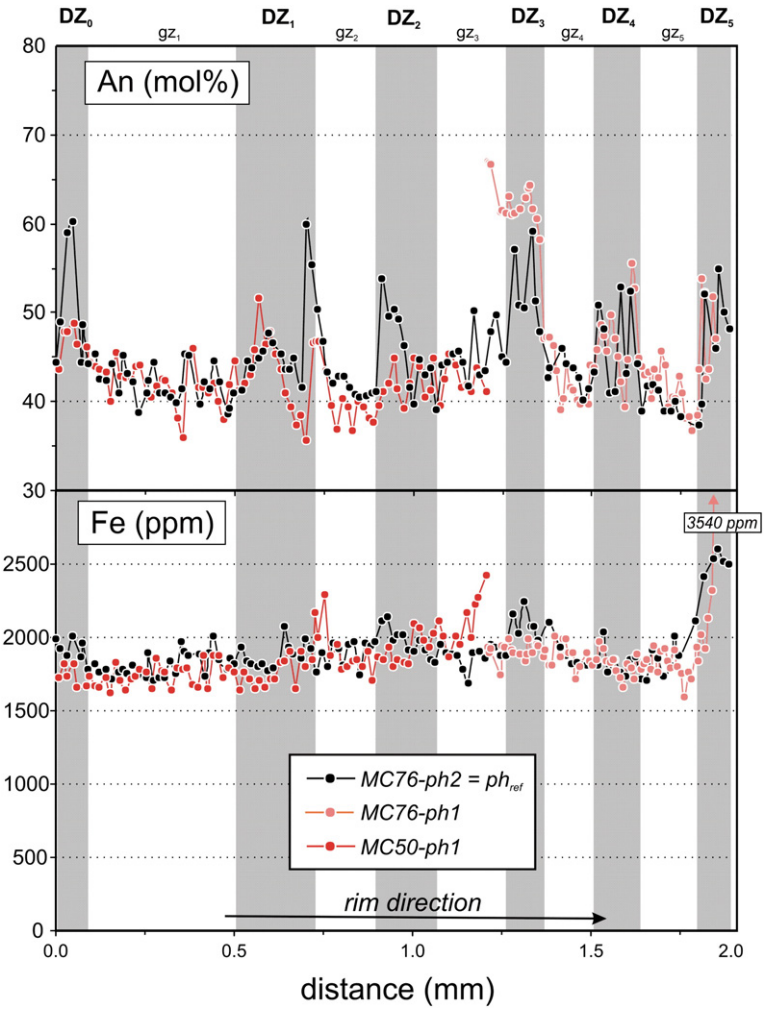

Fig. 9. Correlations between the An and Fe zoning patterns of the Monte Castello plagioclases, i.e., *MC76-ph1*, *MC76-ph2* and *MC50-ph1* investigated in this study. *MC76-ph2* is taken as a reference (=Ph_{ref}) and normalizing frame. The shaded areas correspond to the width of the dissolution zones, which takes into account the MC phenocrysts whose growth histories were correlated in reference to Ph_{ref}.

However, the chemical 'continuity' observed for most elements from [gz4] to [gz5], with particular reference to Fe, indicates that this hypothesis is rather unlikely. Two hypotheses can thus be proposed:

(1) Phenocryst *MC76-ph1* was part of a crystal 'cargo' that crystallized from a separate level of magma differentiation that served as a feeder to a shallower magma chamber (represented by *MC76-ph2*). In this case, the apparent chemical correlation between *MC76-ph1* and *MC76-ph2* (Fig. 9) would only be valid from [DZ_4]. Accordingly, a deeper level of magma differentiation (Stewart and Fowler, 2001; Tomiya and Takahashi, 2005) with less radiogenic $^{87}Sr/^{86}Sr$ may have existed during the first eruptive cycle of the Capraia magma system.

(2) Crystallization of *MC76-ph1* occurred in the lower part of an isotopically- and perhaps compositionally-zoned magma chamber. In this model, [DZ_3] coincides with both the last growth increment recorded in some crystals (*MC50-ph1*) and incipient growth in others (*MC76-ph1*) (Fig. 9). However, the effect of recharge on *MC76-ph2* was only thermal (i.e., pronounced resorption was not followed by a decrease in $^{87}Sr/^{86}Sr$ in the succeeding growth zone), which can be accounted for by growth in upper zones of the magma chamber. Thus, it is possible that phenocryst *MC76-ph2* was resident in the upper zones of the chamber throughout most/all of its crystallisation history. Resorption at [DZ_4] in *MC76-ph1* and *-ph2* may be related to convective overturn in the chamber and efficient mixing, as

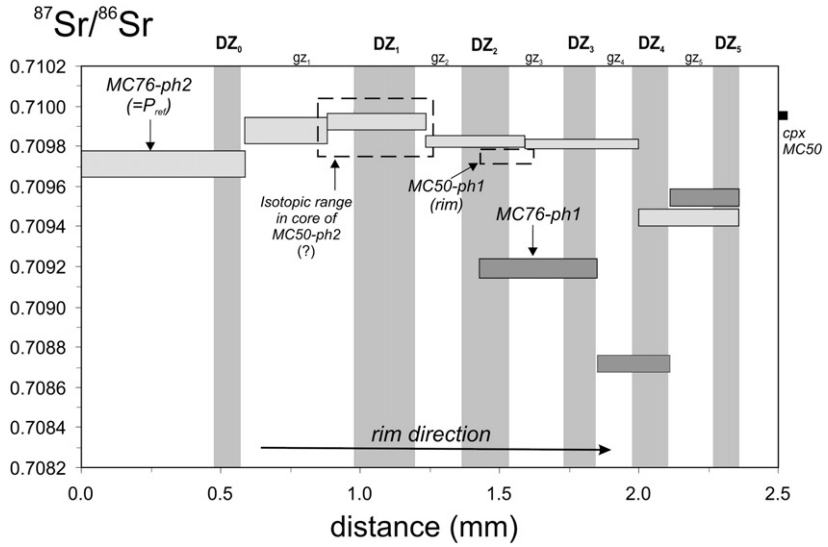

Fig. 10. Correlation between *MC76-ph1* and *MC76-ph2* on the basis of chemical and isotopic data. The shaded areas correspond to the width of the dissolution zones, which takes into account the MC phenocrysts whose growth histories were correlated in reference to Ph_{ref}. Note that that the isotopic composition of the cpx phenocryst analysed in CP50 has isotopic affinities with *MC76-ph2*.

indicated by the similar $^{87}Sr/^{86}Sr$ values in the rim region of both crystals.

Further isotopic data are required to distinguish between these possibilities. The apparent good chemical correlation before [DZ_4] (Fig. 9) despite marked difference in $^{87}Sr/^{86}Sr$ (Fig. 10) may indicate that the replenished magma (hypothesis 1) or the different components co-existing in the magma chamber (hypothesis 2) had similar temperature and fO_2 conditions (which are important control on the An and Fe contents in plagioclase, respectively). A similar discrepancy between the isotopic and chemical zoning information was also reported by Wallace and Bergantz (2005).

The near constant $^{87}Sr/^{86}Sr$ from [gz_1] to [gz_4] in *MC76-ph2* is perhaps surprising, considering that, in crystals inferred to have crystallized from a boundary layer, large An variations often correspond to shifts in isotopic composition after recharge (e.g., Davidson et al., 2001; Charlier et al., 2006). Provided that phenocrysts did not experience much wall-rock contamination (see below), continuous recharge with fresh, hot magma having the same isotopic signature as the resident magma may be able to explain this feature, as well as explain the complicated textures in *MC76-ph2*.

Although isotope data are limited for phenocrysts in dacite MC50, the relatively radiogenic $^{87}Sr/^{86}Sr$ in the rim of *MC50-ph1*, in the resorbed core of *MC50-ph2* and in the clinopyroxene phenocryst have affinities with *MC76-ph2* rather than *MC76-ph1* (Fig. 10), indicating that the radiogenic $^{87}Sr/^{86}Sr$ recharge component may have been dominant during the genesis of the Capraia volcano. Due to its high Fe (>2000 ppm) and $^{87}Sr/^{86}Sr$ (0.70979–0.71002), the patchy-zoned the core of phenocryst *MC50-ph2* (Fig. 4d) may be linked to the [DZ_1] dissolution event (Fig. 10). The original An-rich core (mol% An up to 68) prior to resorption could represent 1) an early episode of growth in the same chamber or 2) be a cognate xenocryst that was introduced into the magma chamber during or following [DZ_1].

The relatively radiogenic Sr recorded in most phenocrysts we have investigated are suggestive of crystallization in a crustally-contaminated boundary layer (Duffield and Ruiz, 1998; Davidson et al., 2001; Tepley and Davidson, 2003). In this case, core-to-rim isotopic variations in *MC76-ph2* should evolve towards more radiogenic compositions as crystallization and contamination by wall-rock proceed. However, this is not observed. Instead, $^{87}Sr/^{86}Sr$ is constant from [gz_1] to [gz_4] (Fig. 7b), suggesting that crustal contamination was not an important process. Rather, intra-grain differences in $^{87}Sr/^{86}Sr$ are interpreted to be related to the different magma components that co-existed in the magma chamber(s). A possible exception is the rimward increase of $^{87}Sr/^{86}Sr$ with decreasing mol% An in the *MC76-ph2* core region (Fig. 7a), which may reveal minor crustal contamination.

The study of the MC plagioclases points to an evolving magma chamber periodically replenished with basaltic to andesitic magmas characterised by variable

$^{87}Sr/^{86}Sr$ signatures. However, the question whether the MR phenocrysts crystallized from the same magma chamber system or in distinct chambers remains open, and has implications for the existence of a large magma body that was progressively tapped during differentiation, i.e. from the MC to the MR dacites. However, the time gap between eruptions (although not well aged-constrained) and markedly different whole-rock trace element signatures for the MR and MC dacites may suggest that they evolved in two separate systems. To resolve this issue, we need to take into account that:

1. MR and MC plagioclases have markedly different Fe contents (Figs. 4 and 5),
2. growth zones in the MR plagioclases are not easily correlated with those in the MC and
3. the MR dacites contain amphibole phenocrysts, whereas the MC dacites do not.

Different Fe contents suggest different temperatures, oxygen fugacity and/or ambient melt compositions when plagioclase crystallization began. Multiple factors control Fe partitioning, but the extent of Fe depletion in plagioclase is generally positively correlated with the degree of Si-enrichment in the melt from which the plagioclase crystallized (Nakada et al., 1994; Hattori and Sato, 1996). Thus, lower Fe in the MR plagioclases is in agreement with growth in more-silicic, water-rich (occurrence of amphibole) and less oxidised melts compared with the MC plagioclases. Although the mean An content overlaps between the MC (42.2±6.5) and MR (45.1±6.0) plagioclases, a closer examination reveals that the number of data points above 40 mol% An is distinctly higher for the MC plagioclases (87% for *MC76-ph1,* 91% for *MC76-ph2*, 74% for *MC50-ph1* and 92% for *MC50-ph2*) than for the MR (50% for *MC20-ph1* and 69% for *MC25-ph1*), which is in agreement with growth of the MR plagioclases in more fractionated, lower temperature, melts. Considering that the cores of *MR20-ph1* and *MC76-ph2* have similar isotopic compositions (Fig. 7b, c; Table 4) and MR and MC phenocrysts have similar mol% An and Sr zonation patterns, we suggest that the MR and MC dacites were likely to have differentiated in the same magma chamber. This is in agreement with the larger size of the MR phenocrysts compared to those in the MC (which were erupted earlier). More fractionated, less-dense melt would tend to buoyantly rise along the wall towards the top of the magma chamber (e.g., Bacon and Druitt, 1988; Sawka et al., 1990). The lack of clear textural and chemical correlations between the MC and MR phenocrysts may be related to different magma dynamics and crystal growth/dissolution controls according to the phenocryst's position in the magma chamber when growth began and/or their time of growth.

The chemical (high mol% An, Sr and Fe; Fig. 5a, b) and isotopic ($^{87}Sr/^{86}Sr>0.710$ in *MR20-ph1*) signatures of the MR plagioclase rims record a distinct magmatic input, which can be correlated with the diagnostically high Sr (>1100 ppm), Ba (>1200 ppm), La (>150 ppm) and radiogenic $^{87}Sr/^{86}Sr$ of the MR dacites (Table 1). This signature is suggestive of a lamproitic end-member. Potassium and silica-rich lamproitic rocks are indeed common in South Tuscany (Peccerillo et al., 1988; Conticelli and Peccerillo, 1992) and also occur in the northern part of the Roman Magmatic Province (e.g., Torre Alfina lavas; Conticelli, 1998). The temperature of the recharge magma was presumably high, in order to account for the extensive biotite breakdown in the resident magma (Fig. 2e).

Generally, radiogenic Sr in most of the MC and MR phenocrysts we have investigated indicates that this lamproitic component was an important, perhaps dominant, end-member in the genesis of the Capraia lavas. However, the typical enriched chemical signature of this component during most of plagioclase crystallization may have been 'diluted' due to the intervention of other processes, such mixing with a less radiogenic component (see above) and crystal fractionation (see below).

10.4. Role of crystal fractionation

The decrease in An content after resorption, predominantly seen in *MC76-ph2* and *MR25-ph1* (see arrows in Figs. 4b and 5c), suggests thermal relaxation after magma recharge compatible with episodes of crystal fractionation, to some extent confirming the whole-rock MFC model suggested by Poli and Perugini (2003). The calculated range of Sr in the melt (Sr_{melt}=200–800 ppm; Fig. 8a) derived from phenocrysts exhibiting the largest range of Sr (in MC76) is somewhat lower than the whole-rock range (494–1184 ppm; Table 1), which indicates that plagioclase fractionation must have heavily scavenged Sr during crystallisation. Fractionation is also consistent with the occurrence of plg–opx–cpx clots, occasional normal zoning in augite and the low temperature estimates (<800 °C). The relatively constant baseline of anorthite content in both MC and MR plagioclases suggests that the amount of melt and heat added after recharge was balanced by release of latent heat during crystallization, which is best accounted for by growth in a crystal-rich boundary layer near the wall and roof of the magma chamber (e.g., Nakada et al., 1994), with possible crystal disruption after recharge (see above). Prolonged

fractionation may have ultimately produced the rhyolitic liquids that were erupted throughout the volcano's history (Fig. 1). For example, eruptions in the Monte Campanile unit produced a significant amount of rhyolitic material (tuff deposits up to 100 m thick) suggesting that a rather large magma chamber may have existed during the first cycle of eruptive activity.

10.5. Role of crystal kinetics

As reported in some cases (Bottinga et al., 1966; Loomis and Welber, 1982; Singer et al., 1995; Ginibre et al., 2002), kinetic processes play an important role during rim growth, where rapid growth enhances partitioning at non-equilibrium conditions due to diffusion processes at the crystal/melt interface. In a plutonic environment, the thermal effect due to magma recharge enhances this effect (Gagnevin et al., 2005a,b). In a volcanic environment, rapid growth is associated with a relative enrichment in incompatible elements and is commonly associated with magma ascent prior to eruption and/or eruptive cooling (Singer et al., 1995; Stewart and Fowler, 2001; Ginibre et al., 2002).

The effect of local kinetics during rim crystallisation in both MC and MR plagioclases is evaluated in the following section. Texturally and chemically, the outer rims differ from one plagioclase to another, although the MR plagioclase rims appear to have a more consistent behaviour than those of MC. Both phenocrysts in MC76 display several resorption events with high An, high Fe and stable Sr concentrations (Fig. 4a, b). Phenocrysts in MC50 exhibit fine oscillations with no significant variations in mol% An and Sr, but as for MC76, Fe increases towards the outer rim (Fig. 4c, d). On the other hand, each of the MR plagioclase rims have high An, Sr and Fe contents (Fig. 5a, b), with the last 20 μm displaying extreme enrichment of Fe (to 5000 ppm). Therefore, while An and Sr abundances are variable, the increase of Fe at the rims is conspicuous and occurs at similar growth stages (<140 μm) for all phenocrysts. Such consistency is expected if rim growth was controlled by interface kinetics during rapid growth (Singer et al., 1995; Ginibre et al., 2002). Crystal-melt interface kinetics favours the incorporation of incompatible elements in the plagioclase lattice (Albarède and Bottinga, 1972). Thus, Fe should be positively correlated with K (D_K<0.1; Philpotts and Schnetzler, 1970). However, the opposite trend is displayed by the MR plagioclase rims (Fig. 11). Thus, kinetic factors must have played only a limited role during rim growth. Instead, the patterns can be interpreted to reflect recharge by a K-poor and Fe-rich magma with a radiogenic Sr isotopic signature (Fig. 7). The MC plagioclase rims plot between these two end-members in K–Fe space, but no systematic relationship is evident (Fig. 11), which also seems to preclude a major role for kinetics during rim growth. Rather, variable An contents in the rims of the MC50 and MC76 phenocrysts suggest that, unlike the MR plagioclases, different magmatic conditions prevailed during rim growth. This is in agreement with the chronological framework detailed earlier (Fig. 9), i.e., phenocryst *MC50-ph1* crystallized earlier than the both

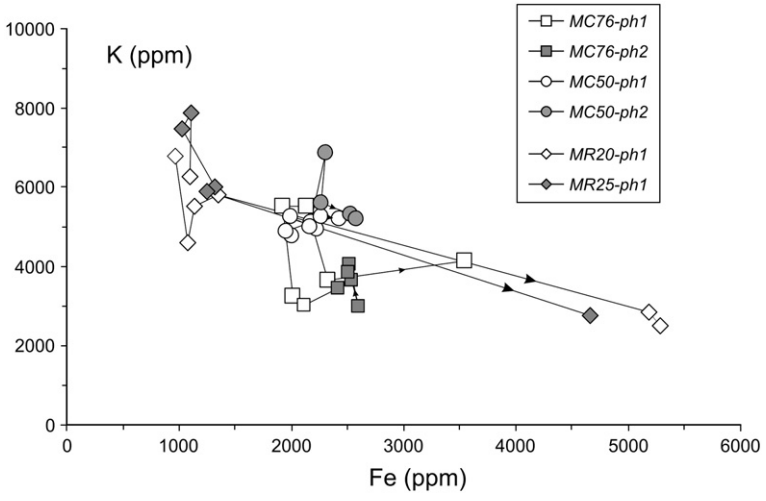

Fig. 11. Fe (ppm) and K (ppm) compositions of MC and MR plagioclase rims (size of the symbols exceeds 1 sigma error). The sense of zoning is shown by the arrows pointing towards the outer rims. The negative correlation (i.e., from the inner to the outer rims) of the MR plagioclase rims is suggestive of magma mixing, with a minor role for crystal kinetics (see text). On the other hand, no clear correlation is observed for the MC plagioclase rims, but magma mixing is nonetheless emphasized on the basis of textural and chemical arguments.

MC76-ph1 and *MC76-ph2*. Lower mol% An fluctuations and weaker resorption features in the MC50 phenocrysts suggest that the rims grew in a quiescent environment, such as in convective cells, where phenocrysts were transported through water-activity and temperature gradients (Singer et al., 1993, 1995; Hattori and Sato, 1996). On the other hand, higher mol% An and pronounced resorption in the MC76 phenocrysts are indicative of a turbulent environment associated with the input of new, mafic magma during rim growth (event [DZ_5]). In this framework, the two successive resorption events in the *MC76-ph2* rim attest to mixing (producing an indented resorption surface), followed by magma ascent prior to eruption (producing a convoluted resorption surface) and simultaneous cooling after eruption (latest stage of growth) (Fig. 4b).

11. Conclusions

This study of plagioclase phenocrysts has provided fresh insight into the open-system behaviour and differentiation history of the Capraia Volcano. Plagioclase phenocrysts in the MC (early) and MR (later) dacites share some textural, chemical and isotopic characteristics, suggesting that they were recycled throughout the entire evolution of the magma system (e.g., Blundy and Shimizu, 1991). Strong isotopic disequilibrium between co-existing plagioclase phenocrysts has been demonstrated on a thin-section scale. Therefore, one cannot make the assumption that the crystallisation history recorded in a single phenocryst is representative of the entire magmatic system. This arises from the fact that magma chambers are dynamic and heterogeneous in space and time, and individually erupted magmas may sample different portions of the space-composition-temperature history.

Remarkably, in spite of clear evidence for chaotic magma dynamics (Perugini et al., 2005), it is possible to identify correlative variations in both chemical and Sr isotopic zoning between separate phenocrysts. By integrating chemical and isotopic data from plagioclase with petrographic evidence, we propose that the MC and MR dacites were erupted from a long-lived (<0.5 Ma; Aldighieri et al., 1998), zoned magma reservoir, with the possible presence of different levels of differentiation. Processes such as influxes of both silicic (Hervig and Dunbar, 1992; Knesel et al., 1999; Waight et al., 2007) and basaltic to trachy-basaltic magmas into lower zones of the chamber (Koyaguchi, 1986; Nakamura, 1995; Feeley and Dungan, 1996; Costa and Singer, 2002), as well as crystallization in a crystal-rich boundary layer (e.g., Nakada et al., 1994) are implied by this study. It is also demonstrated that kinetic factors played a limited role during rim growth. Importantly, this work further underlines the importance of coupling both chemical and isotope data (Feldstein et al., 1994; Tepley et al., 1999, 2000; Halama et al., 2002; Gagnevin et al., 2005a,b; Francalanci et al., 2005) on an intra-grain scale to reconstruct the differentiation history of a magma system, and provides another illustration of the wealth of information derived from the study of even a few phenocrysts.

Acknowledgments

We are grateful to Andreas Kronz for his assistance with the electron microprobe analyses at the Department of Geochemistry, University of Göttingen and to Maurizio Petrelli for carrying out the LA-ICPMS analyses at the Department of Earth-Sciences, University of Perugia. We also thank Gerhard Wörner for the warm welcome in Göttingen. J. Bédard and F. Tepley are acknowledged for their constructive reviews. The Micromill at the Geological Institute, Copenhagen was partially funded by the Carlsberg Foundation. This research was funded by EU contract EVG1-CT-2002-00058 and Science Foundation Ireland (SFI) grant 04/BR/ES0007 awarded to JSD.

Appendix A. Supplementary data

Supplementary data associated with this article can be found, in the online version, at doi:10.1016/j.jvolgeores.2007.07.018.

References

Albarède, F., Bottinga, Y., 1972. Kinetic disequilibrium in trace element partitioning between phenocrysts and host lava. Geochimica et Cosmochimica Acta 36, 141–156.

Aldighieri, B., Gamba, A., Groppelli, G., Malara, F., Pasquare, G., Testa, B., Wijbrans, J., 1998. Methodology for the space-time definition of lateral collapse: the evolution model of Capraia Island (Italy). In: Buccianti, A., Nardi, G., Potenza, R. (Eds.), Proceedings of IAMG '98, the Fourth Annual Conference of the International Association of Mathematical Geology, pp. 79–85.

Andersen, D.J., Lindsley, D.H., Davidson, P.M., 1993. Quilf— a Pascal Program to Assess Equilibria among Fe–Mg–Mn–Ti Oxides, Pyroxenes, Olivine, and Quartz. Computers and Geosciences 19, 1333–1350.

Bacon, C.R., Druitt, T.H., 1988. Compositional evolution of the zoned calcalkaline magma chamber of Mount Mazama, Crater Lake, Oregon. Contributions to Mineralogy and Petrology 98, 224–256.

Barbey, P., Ayalew, D., Yirgu, G., 2005. Insight into the origin of gabbro–dioritic cumulophyric aggregates from silicic ignimbrites: Sr and Ba zoning profiles of plagioclase phenocrysts from Oligocene Ethiopian Plateau rhyolites. Contributions to Mineralogy and Petrology 149, 233–245.

Blundy, J.D., Shimizu, N., 1991. Trace-element evidence for plagioclase recycling in calc-alkaline magmas. Earth and Planetary Science Letters 102, 178–19.

Blundy, J.D., Wood, B.J., 1991. Crystal-chemical controls on the partitioning of Sr and Ba between plagioclase feldspar, silcate melts, and hydrothermal solution. Geochimica et Cosmochimica Acta 55, 193–209.

Bottinga, Y., Kudo, A., Weill, D., 1966. Some observation on oscillatory zoning and crystallisation of magmatic plagioclase. American Mineralogist 51, 792–806.

Brophy, J.G., Dorais, M.J., Donnelly-Nolan, J., Singer, B.S., 1996. Plagioclase zonation styles in hornblende gabbro inclusions from Little Glass Mountain, Medicine Lake volcano, California: implications for fractionation mechanisms and the formation of compositional gaps. Contributions to Mineralogy and Petrology 126, 121–136.

Browne, B.L., Eichelberger, J.C., Patino, L.C., Vogel, T.A., Uto, K., Hoshizumi, H., 2006. Magma mingling as indicated by texture and Sr/Ba ratios of plagioclase phenocrysts from Unzen volcano, SW Japan. Journal of Volcanology and Geothermal Research 154, 103–116.

Brunet, C., Monie, P., Jolivet, L., Cadet, J.P., 2000. Migration of compression and extension in the Tyrrhenian Sea, insights from $^{40}Ar/^{39}Ar$ ages on micas along a transect from Corsica to Tuscany. Tectonophysics 321, 127–155.

Charlier, B.L.A., Ginibre, C., Morgan, D., Nowell, G.M., Pearson, D.G., Davidson, J.P., Ottley, C.J., 2006. Methods for the microsampling and high-precision analysis of strontium and rubidium isotopes at single crystal scale for petrological and geochronological applications. Chemical Geology 232, 114–133.

Clynne, M.A., 1999. A complex magma mixing origin for rocks erupted in 1915, Lassen Peak, California. Journal of Petrology 40, 105–132.

Conticelli, S., 1998. The effect of crustal contamination on ultrapotassic magmas with lamproitic affinity: mineralogical, geochemical and isotope data from the Torre Alfina lavas and xenoliths, Central Italy. Chemical Geology 149, 51–81.

Conticelli, S., Peccerillo, A., 1992. Petrology and geochemistry of potassic and ultrapotassic volcanism in Central Italy: petrogenesis and inferences on the evolution of the mantle sources. Lithos 28, 221–240.

Conticelli, S., Manetti, P., Menichetti, S., 1992. Mineralogy, geochemistry and Sr-isotopes in orendites from South Tuscany, Italy: constraints on their genesis and evolution. European Journal of Mineralogy 4, 1359–1375.

Conticelli, S., D'Antonio, M., Pinarelli, L., Civetta, L., 2002. Source contamination and mantle heterogeneity in the genesis of Italian potassic and ultrapotassic volcanic rocks: Sr–Nd–Pb isotope data from Roman Province and Southern Tuscany. Mineralogy and Petrology 74, 189–222.

Coombs, M.L., Gardner, J.E., 2004. Reaction rim growth on olivine in silicic melts: implications for magma mixing. American Mineralogist 89, 748–758.

Costa, F., Singer, B., 2002. Evolution of Holocene dacite and compositionally zoned magma, Volcan San Pedro, Southern Volcanic zone, Chile. Journal of Petrology 43, 1571–1593.

Couch, S., Sparks, R.S.J., Carroll, M.R., 2001. Mineral disequilibrium in lavas explained by convective self-mixing in open magma chambers. Nature 411, 1037–1039.

Davidson, J.P., Tepley III, F.J., 1997. Recharge in volcanic systems: evidence from isotope profiles of phenocrysts. Science 275, 826–829.

Davidson, J., Tepley III, F., Palacz, Z., Meffan-Main, S., 2001. Magma recharge, contamination and residence times revealed by in situ laser ablation isotopic analysis of feldspar in volcanic rocks. Earth and Planetary Science Letters 184, 427–442.

Dini, A., Innocenti, F., Rocchi, S., Tonarini, S., Westerman, D.S., 2002. The magmatic evolution of the late Miocene laccolith–pluton–dyke granitic complex of Elba Island, Italy. Geological Magazine 139, 257–279.

Duffield, W.A., Ruiz, J., 1998. A model that helps explain Sr-isotope disequilibrium between feldspar phenocrysts and melt in large-volume silicic magma systems. Journal of Volcanology and Geothermal Research 87, 7–13.

Feeley, T.C., Dungan, M.A., 1996. Compositional and dynamic controls on mafic–silicic magma interactions at continental arc volcanoes: evidence from Cordon El Guadal, Tatara–San Pedro Complex, Chile. Journal of Petrology 37, 1547–1577.

Feeley, T.C., Dungan, M.A., Frey, F.A., 1998. Geochemical constraints on the origin of mafic and silicic magmas at Cordon El Guadal, Tatara–San Pedro Complex, central Chile. Contributions to Mineralogy and Petrology 131, 393–411.

Feldstein, S.N., Halliday, A.N., Davies, G.R., Hall, C.M., 1994. Isotope and chemical microsampling: constraints on the history of an S-type rhyolite, San Vincenzo, Tuscany, Italy. Geochimica et Cosmochimica Acta 58, 943–958.

Francalanci, L., Davies, G.R., Lustenhouwer, W., Tommasini, S., Mason, P.R.D., Conticelli, S., 2005. Intra-grain Sr isotope evidence for crystal recycling and multiple magma reservoirs in the recent activity of Stromboli volcano, southern Italy. Journal of Petrology 46, 1997–2021.

Franzini, M., Leoni, L., 1972. A full matrix correction in X-ray fluorescence analysis of rock samples. Atti della Società Toscana di Scienze Naturali, Memorie A79, 7–22.

Gagnevin, D., Daly, J.S., Poli, G., 2004. Petrographic, geochemical and isotopic constraints on magma dynamics and mixing in the Miocene Monte Capanne monzogranite (Elba Island, Italy). Lithos 78, 157–195.

Gagnevin, D., Daly, J.S., Poli, G., Morgan, D., 2005a. Microchemical and Sr isotopic investigation of zoned K-feldspar megacrysts: insights into the petrogenesis of a granitic system and disequilibrium crystal growth. Journal of Petrology 46, 1689–1724.

Gagnevin, D., Daly, J.S., Waight, T.E., Morgan, D., Poli, G., 2005b. Pb isotopic zoning of K-feldspar megacrysts determined by Laser Ablation Multi-Collector ICP-MS: Insights into granite petrogenesis. Geochimica et Cosmochimica Acta 69, 1899–1915.

Ginibre, C., Wörner, G., Kronz, A., 2002. Minor- and trace-element zoning in plagioclase: implications for magma chamber processes at Parinacota volcano, northern Chile. Contributions to Mineralogy and Petrology 143, 300–315.

Gioncada, A., Mazzuoli, R., Milton, A.J., 2005. Magma mixing at Lipari (Aeolian Islands, Italy): insights from textural and compositional features of phenocrysts. Journal of Volcanology and Geothermal Research 145, 97–118.

Giraud, A., Dupuy, C., Dostal, J., 1986. Behaviour of trace elements during magmatic processes in the crust: application to acidic volcanic rocks of Tuscany (Italy). Chemical Geology 57, 269–288.

Halama, R., Waight, T.E., Markl, G., 2002. Geochemical and isotopic zoning patterns of plagioclase megacrysts in gabbroic dykes from the Gardar Province, South Greenland: implications for crystallisation processes in anorthositic magmas. Contributions to Mineralogy and Petrology 144, 109–127.

Harrison, T.M., Watson, E.B., 1984. The behaviour of apatite during crustal anatexis: equilibrium and kinetic considerations. Geochimica et Cosmochimica Acta 48, 1467–1477.

Hattori, K., Sato, H., 1996. Magma evolution recorded in plagioclase zoning in 1991 Pinatubo eruption products. American Mineralogist 81, 982–994.

Hervig, R.L., Dunbar, N.W., 1992. Cause of chemical zoning in the bishop (California) and Bandelier (New Mexico) magma chambers. Earth Planetary Science Letters 111, 97–108.

Hoskin, P.W.O., Kinny, P.D., Wyborn, D., Chappell, B.W., 2000. Identifying accessory mineral saturation during differentiation in granitoid magma: an integrated approach. Journal of Petrology 41, 1365–1396.

Innocenti, F., Serri, G., Ferrara, G., Manetti, P., Tonarini, S., 1992. Genesis and classification of the rocks of the Tuscan Magmatic Province: thirty years after Marinelli's model. Acta Vulcanologica 2, 247–265.

Izbekov, P.E., Eichelberger, J.C., Patino, L.C., Vogel, T.A., Ivanov, B.V., 2002. Calcic cores of plagioclase phenocrysts in andesite from Karymsky volcano: evidence for rapid introduction by basaltic replenishment. Geology 30, 799–802.

Kaye, M.J., 1965. X-ray fluorescence determinations of several trace elements in some standard geochemical samples. Geochimica et Cosmochimica Acta 29, 139–142.

Knesel, K.M., Davidson, J.P., Wendell, A.D., 1999. Evolution of silicic magma through assimilation and subsequent recharge: evidence from Sr isotopes in sanidine phenocrysts, Taylor Creek Rhyolite, NM. Journal of Petrology 40, 773–786.

Koyaguchi, T., 1986. Evidence for two-state mixing in magmatic inclusions and rhyolitic lava domes on Nijima Island, Japan. Journal of Volcanology and Geothermal Research 29, 71–98.

Kuscu, G.G., Floyd, P.A., 2001. Mineral compositional and textural evidence for magma mingling in the Saraykent volcanics. Lithos 56, 207–230.

Lindsley, D.H., 1983. Pyroxene Thermometry. American Mineralogist 68, 477–493.

Longhi, J., Walker, D., Hays, J.F., 1976. Fe and Mg in plagioclase. Proceedings of the Lunar Science Conference, pp. 1281–1300.

Loomis, T.P., Welber, P.W., 1982. Crystallisation processes in the Rocky Hill granodiorite pluton, California: an interpretation based on compositional zoning of plagioclase. Contributions to Mineralogy and Petrology 81, 230–239.

Lundgaard, K.L., Tegner, C., 2004. Partitioning of ferric and ferrous iron between plagioclase and silicate melt. Contributions to Mineralogy and Petrology 147, 470–483.

Morimoto, N., 1988. Nomenclature of Pyroxenes. Bulletin of Mineralogy 111, 535–555.

Murphy, M.D., Sparks, R.S.J., Barclay, J., Carroll, M.R., Brewer, T.S., 2000. Remobilization of andesite magma by intrusion of mafic magma at the Soufrière Hills Volcano, Montserrat, West Indies. Journal of Petrology 41, 21–42.

Nakada, S., Bacon, C.R., Gartner, A.E., 1994. Origin of phenocrysts and compositional diversity in pre-mazama rhyodacite lavas, Crater Lake, Oregon. Journal of Petrology 35, 127–162.

Nakamura, M., 1995. Continuous mixing of crystal mush and replenished magma in the ongoing Unzen eruption. Geology 23, 807–810.

Peccerillo, A., 1999. Multiple mantle metasomatism in central-southern Italy: geochemical effects, timing and geodynamic implications. Geology 27, 315–318.

Peccerillo, A., Poli, G., Serri, G., 1988. Petrogenesis of orenditic and kamafugitic rocks from Central Italy. Canadian Mineralogist 26, 45–65.

Perugini, D., Poli, G., 2000. Chaotic dynamics and fractals in magmatic interaction processes: a different approach to the interpretation of mafic microgranular enclaves. Earth and Planetary Science Letters 175, 93–103.

Perugini, D., Busa, T., Poli, G., Nazzareni, S., 2003. The role of chaotic dynamics and flow fields in the development of disequilibrium textures in volcanic rocks. Journal of Petrology 44, 733–756.

Perugini, D., Poli, G., Valentini, L., 2005. Strange attractors in plagioclase oscillatory zoning: petrological implications. Contributions to Mineralogy and Petrology 149, 482–497.

Philpotts, J.A., Schnetzler, C.C., 1970. Phenocryst–matrix partition coefficients for K, Rb, Sr and Ba, with applications to anorthosite and basalt genesis. Geochimica et Cosmochimica Acta 34, 307–322.

Poli, G., 1992. Geochemistry of Tuscan Archipelago Granitoids, Central Italy: the role of hybridisation processes in their genesis. Journal of Geology 100, 41–56.

Poli, G., Perugini, D., 2003. The Island of Capraia. In: Poli, G., Perugini, D., Rocchi, S., Dini, A. (Eds.), Miocene to recent plutonism and volcanism in the Tuscan Magmatic Province (Central Italy). Periodico di Mineralogia, vol. LXXII(2), pp. 195–200.

Prosperini, N., 1993. Petrologia e geochimica delle rocce dellisola di Capraia (Arcipelago Toscano, Italia): un vulcano calcalcalino di origine complessa. MSc Thesis, University of Perugia, Italy, 223 pp.

Price, R.C., Gamble, J.A., Smith, I.E.M., Robert, B., Stewart, R.B., Eggins, S., Wright, I.C., 2005. An integrated model for the temporal evolution of andesites and rhyolites and crustal development in New Zealand's North Island. Journal of Volcanology and Geothermal Research 140, 1–24.

Sawka, W.N., Chappell, B.W., Kistler, R.W., 1990. Granitoid compositional zoning by side-wall boundary layer differentiation: evidence from the Palisade Intrusive suite, Central Sierra Nevada, California. Journal of Petrology 31, 519–553.

Schmitt, A.K., de Silva, S.L., Trumbull, R.B., Emmermann, R., 2001. Magma evolution in the Purico ignimbrite complex, northern Chile: evidence for zoning of a dacitic magma by injection of rhyolitic melts following mafic recharge. Contributions to Mineralogy and Petrology 140, 680–700.

Serri, G., Innocenti, F., Manetti, P., 1993. Geochemical and petrological evidence of the subduction of delaminated Adriatic lithosphere in the genesis of the Neogene–Quaternary magmatism of central Italy. Tectonophysics 223, 117–147.

Shimizu, N., Le Roex, A.P., 1986. The chemical zoning of augite phenocrysts in alkaline basalts from Gough Island, South Atlantic. Journal of Volcanology and Geothermal Research 29, 159–188.

Singer, B.S., Pearce, T.H., Kolisnik, A.M., Myers, J.D., 1993. Plagioclase Zoning in mid-Pleistocene Lavas from the Seguam Volcanic Center, Central Aleutian Arc, Alaska. American Mineralogist 78, 143–157.

Singer, B.S., Dungan, M.A., Layne, G.D., 1995. Textures and Sr, Ba, Mg, Fe, K and Ti compositional profiles in volcanic plagioclase: clues to the dynamics of calc-alkaline magma chambers. American Mineralogist 80, 776–798.

Smith, J.V., Brown, W.L., 1988. Feldspar Minerals. 1, crystal structures, physical, chemical and microtextural properties. Springer Verlag. 828 pp.

Stewart, M.L., Fowler, A.D., 2001. The nature and occurrence of discrete zoning in plagioclase from recently erupted andesitic volcanic rocks, Montserrat. Journal of Volcanology and Geothermal Research 106, 243–253.

Stimac, J.A., Pearce, T.H., 1992. Textural evidence of mafic–felsic magma in dacite lavas, Clear Lake, California. American Mineralogist 77, 795–809.

Tepley III, F.J., Davidson, J.P., 2003. Mineral-scale Sr-isotope constraints on magma evolution and chamber dynamics in the Rum layered intrusion, Scotland. Contribution to Mineralogy and Petrology 145, 628–641.

Tepley III, F.J., Davidson, J.P., Clynne, M.A., 1999. Magmatic interactions as recorded in plagioclase phenocrysts of Chaos Crags, Lassen Volcanic Center, California. Journal of Petrology 40, 787–806.

Tepley III, F.J., Davidson, J.P., Tilling, R.I., Arth, J.G., 2000. Magma mixing, recharge and eruption histories recorded in plagioclase phenocrysts from El Chichon volcano, Mexico. Journal of Petrology 41, 1397–1411.

Thompson, K.A., Dungan, M.A., 1985. The petrology and geochemistry of the Handkerchief Mesa mixed magma complex, San Juan Mountains, Colorado. Journal of Volcanology and Geothermal Research 26, 251–274.

Tomiya, A., Takahashi, E., 2005. Evolution of the magma chamber beneath Usu Volcano since 1663: a natural laboratory for observing changing phenocryst compositions and textures. Journal of Petrology 46, 2395–2426.

Triebold, S., Kronz, A., Wörner, G., 2006. Anorthite-calibrated backscattered electron profiles, trace elements, and growth textures in feldspars from the Teide–Pico Viejo volcanic complex (Tenerife). Journal of Volcanology and Geothermal Research 154, 117–130.

Troll, V.R., Schmincke, H.U., 2002. Magma mixing and crustal recycling recorded in ternary feldspar from compositionally zoned peralkaline Ignimbrite 'A', Gran Canaria, Canary Islands. Journal of Petrology 43, 243–270.

Tsuchiyama, A., 1985. Dissolution kinetics of plagioclase in the melt system diopside–albite–anorthite, and origin of dusty plagioclase in andesite. Contributions to Mineralogy and Petrology 89, 1–16.

Umino, S., Horio, A., 1998. Multistage magma mixing revealed in phenocryst zoning of the Yunokuchi Pumice, Akagi volcano, Japan. Journal of Petrology 39, 101–124.

Van Bergen, M.J., 1985. Common trace-element characteristics of crustal- and mantle-derived K-rich magmas at Mt. Amiata (central Italy). Chemical Geology 48, 125–135.

Waight, T.E., Maas, R., Nicholls, I.A., 2000. Fingerprinting feldspar phenocrysts using crystal isotopic composition stratigraphy: implications for crystal transfer and magma mingling in S-type granites. Contributions to Mineralogy and Petrology 139, 227–239.

Waight, T.E., Wiebe, R.A., Krogstad, E.J., 2007. Isotopic evidence for multiple contributions to felsic magma chambers: Gouldsboro granite, coastal Maine. Lithos 93, 234–247.

Wallace, G.S., Bergantz, G.W., 2004. Constraints on mingling of crystal populations from off-center zoning profiles: a statistical approach. American Mineralogist 89, 64–73.

Wallace, G.S., Bergantz, G.W., 2005. Reconciling heterogeneity in crystal zoning data: an application of shared characteristic diagrams at Chaos Crags, Lassen Volcanic Center, California. Contributions to Mineralogy and Petrology 149, 98–112.

Watson, E.B., Harrison, T.M., 1983. Zircon saturation revisited: temperature and composition effects in a variety of crustal magma types. Earth and Planetary Science Letters 64, 295–304.

Wilke, M., Behrens, H., 1999. The dependence of the partitioning of iron and europium between plagioclase and hydrous tonalitic melt on oxygen fugacity. Contributions to Mineralogy and Petrology 137, 102–114.

Zellmer, G.F., Sparks, R.S.J., Hawkesworth, C., Wiedenbeck, M., 2003. Magma emplacement and remobilization timescales beneath Montserrat: insights from Sr and Ba zonation in plagioclase phenocrysts. Journal of Petrology 44, 1413–1431.